https://doi.org/10.5194/egusphere-2025-5841
Preprint. Discussion started: 9 December 2025

AI based seasonal large ensembles for fluvial flood risk: Evaluation over the Elbe basin

John Ashcroft[1,*], Alison Poulston[1,*], Marius Koch[2], Georg Ertl[2], Kirsty Brown[1], James Butler[1], Anthony Hammond[3], Owen Jordan[1], Sarah Warren[3], Rob Lamb[4,5], Paul J. Young[1,6], and David Wood[1]

[1]JBA Risk Management, Skipton, BD23 3FD, United Kingdom
[2]Nvidia Corporation, 2788 San Tomas Expressway Santa Clara, CA 95051, USA
[3]JBA Consulting, Skipton, BD23 3FD, United Kingdom
[4]JBA Trust, Skipton, BD23 3FD, United Kingdom
[5]Lancaster Environment Centre, Lancaster University, Lancaster, LA1 4YQ, United Kingdom
[6]School of Engineering, Newcastle University, Newcastle, NE1 7RU, United Kingdom

[*]These authors contributed equally to the manuscript

Correspondence to: john.ashcroft@jbarisk.com

Abstract.

A key challenge in risk analysis is to identify hazard events that are plausible and yet extrapolate beyond historical observations with appropriate frequency. For flood risk management, this can be done with large ensembles of synthetic, physically plausible weather scenarios that extend beyond the historical record to sample low-likelihood, high-impact events. Traditional statistical approaches for synthetic weather generation are often limited in variability and physical realism. Here, we show for the first time that a machine learning weather prognostic model, combined with a diagnostic precipitation model, can generate seasonal-scale ensembles suitable for flood risk assessment. Specifically, we adapt the huge ensembles (HENS) approach using a Spherical Fourier Neural Operator (SFNO)-based model combined with an Adaptive Fourier Neural Operator (AFNO)-based diagnostic precipitation model, using Nvidia Earth-2 stack, in a framework which we call "PrecipHENS", to produce >1000 synthetic European winter seasons of precipitation and temperature at 0.25° resolution in 112 GPU hours on NVIDIA L40s GPUs. In an Elbe River case study, PrecipHENS reproduces key features of the precipitation and temperature climatology, preserves spatial and temporal dependence – including decay of extremal co-occurrence with distance – and generates a wider diversity of extreme events than an industry-standard conditional multivariate extreme value model benchmark. Principal component analysis of extreme precipitation fields shows that PrecipHENS spans a much broader space of storm structures (≈81% of 1×1 grid cells) than the benchmark (≈50%) or the historical record (≈19%), indicating plausible novelty rather than repetition of past patterns. Coupled with a hydrological model, the AI-generated weather sequences produce river flow simulations consistent with historical climatology and extreme discharge patterns. These results demonstrate the potential of AI-based weather models to support event set generation for flood hazard and risk applications. Beyond flood risk, such AI-based large-ensemble weather generation offers a general framework for applications that benefit from expanding the physically plausible sample space, including risk assessment, climate-impact analysis, storyline development and statistical characterisation of extremes.

1. Introduction

Flooding is a complex and damaging natural hazard, with both pluvial (surface water) and fluvial (riverine) events contributing to substantial financial, environmental, and social costs (Svetlana et al., 2015; Allaire, 2018; Zhang et al., 2024). For example, CRESTA CLIX (2024) described 2024 as the 'year of the flood', with flood events responsible for 78% of the US $18.2 billion in insured losses from all non-US catastrophe events exceeding US $1 billion. Estimating flood risk is crucial for disaster preparedness, infrastructure planning, and insurance modelling (Mitchell-Wallace et al., 2017; Tyler et al., 2019; Ferreira et al., 2022; Lamb et al., 2022), yet remains challenging because floods are highly variable in space and time, span a wide range of scales, and many observational records are short and incomplete.

To overcome these challenges, flood risk estimation often relies on simulation-based approaches that generate large sets of synthetic but physically plausible weather scenarios, extending the effective sample of hydrometeorological extremes. In catastrophe models, which are particularly used in the insurance and reinsurance industries, these "event sets" underpin probabilistic estimates of losses from pluvial and fluvial flooding (Mitchell-Wallace et al., 2017). Each event set comprises of spatially and temporally coherent weather and hydrological patterns, typically precipitation fields for pluvial flooding and river flow simulations for fluvial flooding, that together represent the diversity of potential flood events.

One strategy for event set simulation is to adopt physics-based models, which may be nested to achieve the required spatial scales for flood impacts analysis (Cotterill et al., 2024; Kay et al., 2018; Schaller et al., 2016). Such approaches provide a physically consistent means of exploring rare events beyond the observed record, but they remain computationally expensive and constrained by model resolution. An alternative is to use statistical techniques based on parametric multivariate extreme-value models trained on historical data (Keef et al., 2013). This approach lacks representation of physical dynamics but is computationally efficient, draws on direct inference from extreme event observations, and can reproduce observed spatial and temporal dependencies and marginal extremes without necessarily covering the entire sample space of plausible spatial weather patterns.

In contrast, new AI-based weather models offer the potential to generate realistic weather data at low computational cost while capturing complex spatial and temporal dynamics (Mahesh et al., 2024a). This study explores this new potential by evaluating whether an AI-powered weather model can generate seasonal ensembles of weather data that are fit for purpose as event set inputs for flood risk analysis. Specifically, we (i) compare AI-generated precipitation against an established industry benchmark based on multivariate extreme value theory, and (ii) assess the hydrological implications of the AI simulations by converting them to river flows using a conceptual hydrological model. The remainder of the introduction explains these two components in more detail.

1.1 Precipitation generation

1.1.1 Benchmark approach

Our benchmark statistical method models the marginal distributions and dependence structure of observed extremes to produce long records over thousands of simulated years of statistically plausible events. Using historical data, statistical methods model the correlation structure – particularly that of extremes – with conditional multivariate parametric extreme value models (Heffernan and Tawn, 2004), Gaussian copula-based approaches (Alexandre et al., 2024; Brunner et al., 2019; Lee and Joe, 2018), signal-based transformations (Brunner et al., 2020; Brunner and Gilleland, 2020; Van De Vyver, 2024), and dimension reduction techniques such as principal components analysis (Cooley and Thibaud, 2019; Drees and Sabourin, 2021; Rohrbeck and Cooley, 2022). While effective, many of these methods become computationally demanding at large spatial scales, and, except for Heffernan and Tawn (2004), assume a fixed form of tail dependence, which can lead to biased risk estimates (Lamb et al., 2010; Tawn et al., 2018). In contrast, observed precipitation often shows mixed tail behaviour, with extremal co-occurrence weakening at the highest levels (Keef et al., 2009).

In this study we adopt the conditional multivariate framework of Heffernan and Tawn (2004) as the benchmark. It is widely used in industry and research for flood risk applications (Formetta et al., 2024; Lamb et al., 2010; Li et al., 2023; Olcese et al., 2024; Sando et al., 2024; Towe et al., 2018; Wang et al., 2024) and it can flexibly represent spatial tail dependence at large spatial scales (Keef et al., 2009). The benchmark approach has been adapted for both direct river flow estimation (Keef et al., 2013; Lamb et al., 2010; Quinn et al., 2019) and for precipitation modelling that is then used as input to hydrological simulation (Brocca et al., 2011). Here, we use its precipitation-generation configuration to provide a like-for-like comparison with the AI-generated weather data.

1.1.2 AI weather model

Physics-based simulators can decouple from initial conditions over long lead times but are constrained by resolution and the computational cost of a large ensemble. Machine learning emulators of these physical simulations offer faster runtimes but often under-represent extremes because standard training objectives, such as minimising mean-squared error, encourage the model to reproduce average conditions rather than the full range of variability (Mahesh et al., 2024a; Xu et al., 2024). The Spherical Fourier Neural Operator (SFNO) has recently shown promise for stable, long roll outs (Bonev et al., 2023) and to retain realistic variability, including extremes, in ensemble applications (Mahesh et al., 2024a, b). Although SFNO is deterministic, ensemble diversity can be introduced by varying initial conditions and model checkpoints. The resulting simulations are not predictive in the forecast sense but are plausible evolutions valuable for risk estimation because they expand the set of rare conditions beyond those observed.

1.1.3 Precipitation goals

Here we test such an SFNO-based framework for stochastic weather generation relevant to flood risk estimation and compare it directly against the benchmark. For hydrologically meaningful tail risk estimates, synthetic weather generation must satisfy four key goals, which we label G1–G4 and describe below.

G1. Preservation of observed climatology, which involves reproducing key climatic features, such as long-term means, seasonal cycles, and statistical distributions of variables like precipitation. This is particularly important for conceptual hydrological models, such as the model we will use later, which integrate water balances over time and are sensitive to biases in meteorological inputs.

G2. Realistic spatial and temporal coherence, which requires that simulations reflect realistic spatial and temporal dependencies. Inadequate representation leads to fragmented or overly smooth precipitation fields, distorting event sequencing and persistence. Coherence must be maintained both in typical variability and in rare events, which are especially relevant for catastrophe modelling where risk is aggregated across time (e.g., insurance terms) and space (e.g., national portfolios) (Lamb et al., 2010; Mitchell-Wallace et al., 2017). Event clustering and spatial structure matter both for long-term patterns (e.g. seasonal drivers) and short-term impacts (e.g. flooding across catchments) (Merz et al., 2014; Steirou et al., 2022).

G3. Realistic representations of extreme events, which highlights the importance of simulating the frequency and magnitude of extremes. Under- or overestimating the tails of the distribution can respectively underplay or exaggerate risk. While global datasets such as ERA5 (Hersbach et al., 2020) offer useful historical context, their limited length challenges the simulation of long return period events.

G4. Methodological robustness and generalisability, which refers to the need for variability without overfitting and demonstrating controlled sensitivity to changes in input conditions. This is vital given the spatial heterogeneity of flood drivers; events are often locally unique due to terrain, land use, and hydrological conditions and thus generally not transferable to another location (Zanardo and Salinas, 2022).

1.2 River flow generation

While precipitation simulations allow direct assessment of pluvial flooding, river flow is the key variable for fluvial risk. Given a weather simulation, a continuous hydrological simulation translates precipitation and temperature – interacting with soil moisture, snow processes, and catchment characteristics – into streamflow. Because the AI-based framework produces both precipitation and temperature, we can evaluate whether its fully correlated hydrometeorological inputs produce credible river-flow responses, using the same goals (G1–G4) as for precipitation. These flows can then be used in hydraulic modelling or statistical severity analysis, enabling consistent flood risk estimation across pluvial and fluvial event types.

1.3 Outline of the paper

We demonstrate, for the first time, that an AI-powered weather model can generate seasonal ensembles suitable for event set creation in flood risk estimation by evaluating against G1–G4 above. Section 2 Data and methods details the data and methods, including the SFNO-based framework (Mahesh et al., 2024a, b) and our benchmark. The results in Section 3 Results first assess the two simulation approaches against G1–G4 for precipitation over a large European river basin before presenting a method to translate these sequences into river flow, evaluated against the same criteria. We conclude in Section 4 Discussion and conclusion with a discussion of the broader implications of this proof-of-concept study for the flood risk industry.

2 Data and methods

2.1 Data

2.1.1 Geographical region of study

The analysis in this study focuses on the Elbe river basin in Germany (Figure 1), a large European catchment that encompasses varied geomorphological conditions from the mountainous upper catchment in Czech Republic to its lowland floodplains in Germany. The Elbe is susceptible to basin-wide winter flooding (Merz and Thieken, 2009) due to a combination of direct rainfall and snowmelt (Nied et al., 2013), making it a testing demonstration case because the co-occurrence of these processes exposes the interdependence between precipitation and temperature.

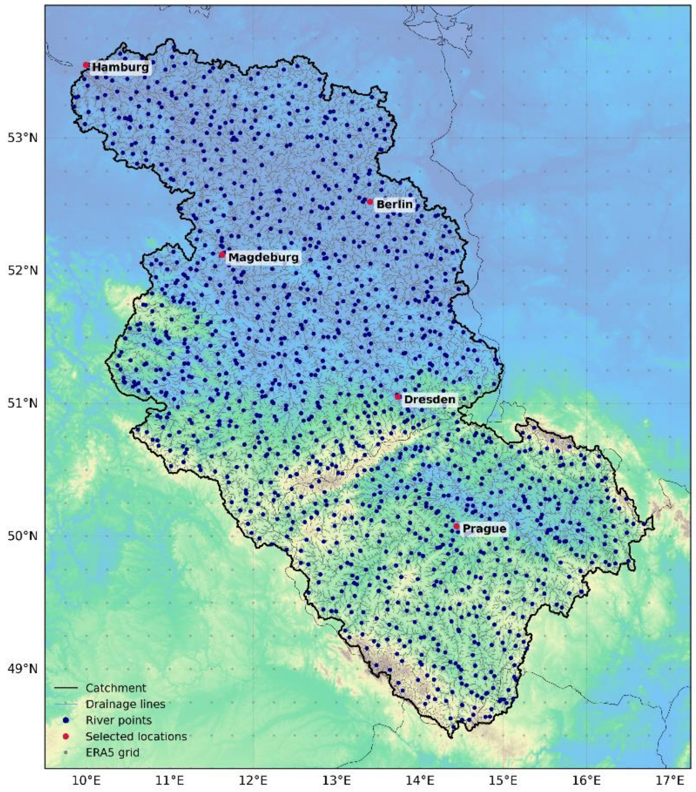

Figure 1: Overview map of the Elbe River basin showing the catchment outline (black), drainage lines (grey), river simulation points (blue), and the ERA5 reanalysis grid (light grey). Some selected major cities (red) are labelled for geographical reference. Terrain shading derived from the Copernicus GLO-30 Digital Surface Model highlights topographic variation across the region.

2.1.2 Historical atmospheric variables

All historical atmospheric data in this study are derived from ECMWF Reanalysis v5 (ERA5) (Hersbach et al., 2020). The inputs to the AI-powered model are the 74 atmospheric variables for the eight lagged initial dates, all taken at 00hrs (see Mahesh et al (2024a) for the full variable list).

The statistical benchmark approach (Section 2.2.1 Benchmark approach) requires a historical period from which to fit both the marginal extreme precipitation model and the large-scale extreme frequency and region model. Here we used the years 1980–2024, taken from ERA5 but passed through the diagnostic model used within the AI-workflow (Precipitation AFNO) (Pathak et al., 2022). This allowed more direct comparison between the simulated weather from the two approaches without needing to account for biases between ERA5 and Precipitation AFNO. Hereafter, all references to “historical data” denote ERA5 2 m temperature and precipitation obtained from the diagnostic Precipitation AFNO model forced with ERA5 inputs. Data were aggregated to daily resolution by averaging temperature and summing precipitation.

https://doi.org/10.5194/egusphere-2025-5841
Preprint. Discussion started: 9 December 2025

2.1.3 Historical river data

Flow was analysed across multiple catchments in the Elbe region, encompassing both gauged and ungauged locations. Observed discharge data from gauged sites are required for the calibration of the hydrological model (GR4J, see Section 2.3 River flow generation methodology), and daily observed river flow data covering 1981–2017 for the Elbe region was sourced from Large Sample Data for Hydrology and Environmental Sciences for Central Europe (LamaH-CE; Klingler et al., 2021), although many of the catchments contain incomplete records.

Catchments were delineated from a 25m hydrologically conditioned digital elevation model (DEM), derived from the Copernicus EU-DEM (European Environment Agency (EEA), 2016) and national lidar datasets. High-resolution lidar data were resampled and feathered to ensure seamless integration with the continental DEM, providing a consistent terrain surface across Europe. Sinkholes were clipped and major drainage lines (>500 km^2 contributing area) from JBA's Global Flood Map (Thornton et al., submitted) were hydrologically forced into the DEM to enforce realistic flow routing.

The conditioned DEM was processed using version 1.4 of the SCALGO Hydrology software (Scalgo Hydrology, n.d.) to derive flow directions, drainage networks, and nested catchment boundaries through sequential flooding, flow routing and watershed modules. Approximately 20000 station points were generated along drainage lines with higher densities in urban areas, supplemented by gauged sites from LamaH-CE. Gauged catchments were validated by comparing SCALGO-derived catchment areas with documented drainage areas of flow gauges, with discrepancies exceeding 20% manually reviewed and reclassified as ungauged where appropriate. Catchments within the Elbe River basin were then selected from this continental dataset. The final dataset comprises 68 gauged and 1294 ungauged catchments (shown in Figure 1). Attributes describing catchment characteristics used to facilitate the prediction in ungauged basins are extracted from several global-scale datasets described in Table A1.

2.2 Precipitation generation methodology

We generated stochastic daily timeseries of precipitation at a spatial resolution of 0.25 degrees using the benchmark and AI approaches. For both approaches, we targeted an ensemble of approximately 1000 independent 3-month long periods that capture December, January, and February (i.e., the European winter period).

2.2.1 Benchmark approach

We implemented an extension of the methodology of Keef et al (2013), which has been widely used both in practice (Olcese et al., 2024; Quinn et al., 2019; Towe et al., 2018) and for academic studies (Lamb et al., 2010, 2019). This is a hybrid simulation technique that captures the underlying climatology via statistical bootstrapping and extremes via a conditional multivariate extremal dependence model (Figure 2).

https://doi.org/10.5194/egusphere-2025-5841
Preprint. Discussion started: 9 December 2025

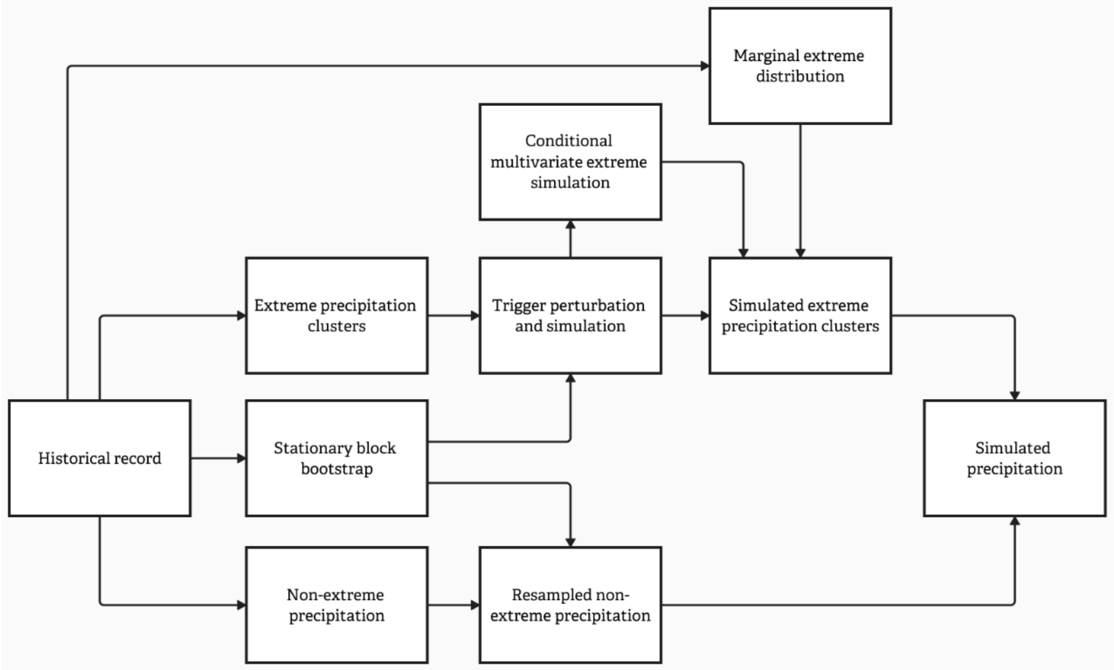

Figure 2: Schematic of the benchmark approach to weather generation. The method combines a stationary block bootstrap for non-extreme precipitation with a conditional multivariate extreme-value model for extremes. Extreme precipitation clusters are perturbed using historical dependence structures, then merged with resampled non-extreme precipitation to produce full synthetic precipitation fields.

Precipitation extremes were modelled by treating storms as spatiotemporal clusters and first considering the long-range dependency structure (the spatiotemporal model of clusters) and, conditional on this, the short-range dependency structure (the spatiotemporal evolution within the cluster). Precipitation at any location was regarded as extreme on any day that it exceeds the 99th percentile of the historical record at that location. Extreme instances were grouped into clusters by considering sequential runs of days and a spatial distance threshold (Davison and Smith, 1990). Here, we allowed a single cluster to have up to a single day break temporally and a 350km break spatially. Both thresholds were chosen based on a regional study of the tail dependence in historical precipitation; tail dependence was calculated for a range of temporal lags and distance thresholds and an elbow point across the region of study was determined at which the dependence decayed (Ledford and Tawn, 1996). The long-range structure of precipitation is modelled as a spatiotemporal point process. The size of the spatiotemporal domain considered prohibits a parametric point process under the limited historical data record (Keef et al., 2013), and so a non-parametric stationary block bootstrap model was used (Politis and Romano, 1994). Stationary block bootstrapping resamples the historical data from a uniform multinomial model, retaining annual blocks. To capture both inter- and intra-year variability, the block length was varied, with such length following a Poisson distribution with the unit being the number of years. The resampled blocks at an annual scale are joined at the beginning of the month with the fewest precipitation clusters to minimise discontinuity (in this case, February). Our focus is on an ensemble of independent winter seasons, and we generated 1000 resampled blocks of 3-months, each of which can either be from a single coherent historical year or from a disjoint pair of historical years straddling January and February. The long-range structure of the simulated precipitation is thereby defined by the block-bootstrap, with the frequency and region of extreme clusters being that in the resampled data.

The short-range structure of precipitation was modelled using a perturbation scheme coupled with the conditional multivariate extremal dependence model (Heffernan and Tawn, 2004; Ledford and Tawn, 1996). The cluster trigger was defined as the location with the highest quantile of precipitation on the first day. New clusters were simulated by first perturbing the trigger location, simulating the precipitation at the trigger, and then conditionally simulating the precipitation at all remaining locations and times in the cluster. The perturbation follows a transition probability field defined by Ledford and Tawn (1996) which represents the conditional probability that a location becomes the trigger given that a trigger has been observed at another location. It has been shown to capture the influence of both distance and topography on precipitation dependence effectively (Keef et al., 2009, 2013). For each resampled extreme cluster, a new trigger is simulated according to this probability field, and an extreme quantile is simulated uniformly. The conditional multivariate extremal dependence model (Heffernan and Tawn, 2004) was used to simulate the quantiles of precipitation at all other locations and times in the resampled cluster, dependent on the perturbed trigger and with an extreme covariance structure defined by that of the historical cluster. Simulated quantiles of precipitation are converted to actual precipitation via marginal extreme value distributions fitted independently to historical data at each location, thereby preserving spatial variations in the precipitation climatology as the cluster severity is resampled.

2.2.2 PrecipHENS: AI-powered approach

We assess the potential of AI-powered weather generation by following the huge ensembles (HENS) approach, which demonstrates competitive performance against operational weather forecast systems (Mahesh et al., 2024a, b). HENS employs ensemble methods traditionally used in numerical weather prediction to explore two major sources of uncertainty in the forecasts: the initial conditions and the forecast model. HENS accounts for initial condition uncertainty through a custom centred bred vector perturbation scheme (Mahesh et al., 2024a; Toth and Kalnay, 1993, 1997). This scheme samples the fastest-growing modes of forecast error by iteratively breeding perturbations through the model dynamics, generating flow-dependent perturbations that maintain physically consistent structures across variables and levels.

The forecast model applied in HENS is a tailored version of SFNO (Bonev et al., 2023), a machine learning emulator of global numerical reanalyses, here trained on ERA5 from 1979–2016 (Hersbach et al., 2020). SFNO is well suited for producing (sub)seasonal predictions as it has been shown to be stable for such rollout lengths and to follow the seasonal cycle (Karlbauer et al., 2024). For HENS, the architecture and the training methodology of SFNO have been configured for improved representation of extremes. SFNO is a deterministic forecast model and therefore lacks an inherent representation of model uncertainty. To approximate this, the developers trained multiple model "checkpoints" using identical training data and protocols but different random initialisations, causing each checkpoint to converge to a distinct local minimum of the mean-squared-error loss surface used during training and so providing a diverse ensemble of plausible solutions.

The data generated by HENS consists of 74 surface and pressure level variables provided on a 0.25° horizontal grid and 13 vertical pressure levels but does not include precipitation. However, total accumulated precipitation can be derived from the HENS prediction through a diagnostic machine learning model (Pathak et al., 2022) based on the Adaptive Fourier Neural Operator architecture. Hereafter we refer to the full pipeline of HENS with diagnostic precipitation model as PrecipHENS. We implemented PrecipHENS based on the huge ensemble workflow in NVIDIA's earth2studio library (PhysicsNeMo Contributors, 2024).

For the current study, we generated a 1008-member ensemble, with each member simulated over 115 days spanning the 3-month winter period (Figure 3). A set of eight lagged initial conditions were used from 9–16 November 2023, inclusive, with each initial condition being taken at 00hr from ERA5. Initial conditions were chosen from mid-November to allow at least two weeks for the simulation to decouple from its initial conditions (Mahesh et al., 2024a). For each initial condition, an unperturbed version was input to the model, along with four pairs of bred vector perturbations (each perturbation pair being an addition and subtraction), creating nine perturbation instances for each lagged initial time and a total of 72 unique initial conditions. A random subset of 14 available checkpoints from the HENS study were used, with each checkpoint running the 72 initial conditions, thus creating the 1008-member ensemble. For the results in this study, only the data from December onwards was retained, and the 6-hourly simulations were aggregated to daily with each day being from the 00hr timestep.

PrecipHENS was generated on NVIDIA L40s GPUs with a batch size of two members per GPU. The rollout for two ensemble members takes on average 13 minutes 20 seconds, i.e., requiring roughly 112 GPU hours to produce the full precipitation dataset. Since the ensemble members are only correlated to one other ensemble member with opposite perturbation vector for initial conditions, but are independent otherwise, data generation could be parallelised across the ensemble dimension.

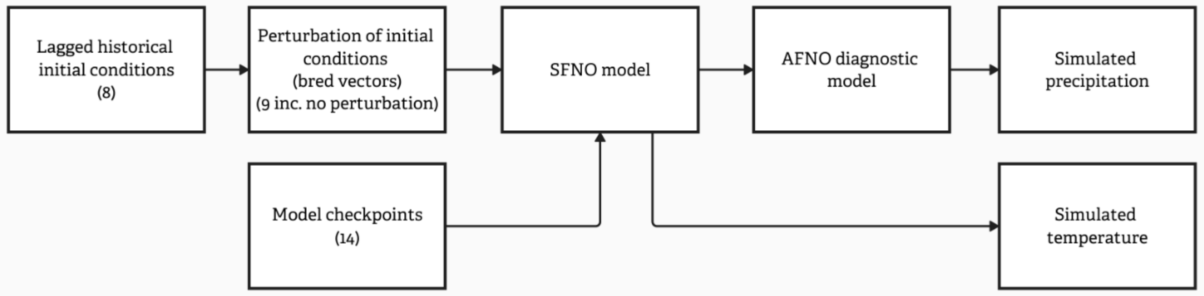

Figure 3: Schematic of PrecipHENS, the AI-powered approach to weather generation we develop in this study. Lagged historical initial conditions are perturbed using bred vectors and passed through multiple SFNO model checkpoints to represent initial condition and model uncertainty. The SFNO forecasts are then processed through an AFNO-based diagnostic model to generate simulated precipitation and temperature.

2.3 River flow generation methodology

We simulated river flows produced by each weather ensemble member using the GR4J model (Perrin et al., 2003), which is a lumped conceptual rainfall-runoff model with a small number of parameters that relate to physical catchment properties and to inputs of precipitation and potential evapotranspiration. GR4J provides a flexible, conceptual rainfall-runoff model representation that is well accepted in flood risk and water resource management (Kunnath-Poovakka and Eldho, 2019; Shin and Kim, 2017).

As implemented here, GR4J models each catchment draining to the simulation points shown in Figure 1 independently (as opposed to an explicit routing model or semi-distributed implementation), although the catchments are nested to implicitly instil correlation from upstream to downstream. The gridded weather data – generated as described in Section 2.2 Precipitation generation methodology – was aggregated across each catchment, taking the mean precipitation and temperature within the catchment boundary. In the rare case that a catchment boundary is too small to include a grid cell (for very small, upstream catchments), an inverse distance weighting scheme was used based on the four nearest grid cell centres. The temperature was converted to potential evapotranspiration following the method of Oudin et al (2005). The six-parameter Cemaneige snow model extension to GR4J (Valéry et al., 2014a, b) is used for catchments where the temperature is below freezing for more than 10% of the year, with this threshold having been chosen to provide a pragmatic balance between unnecessary computation of the snow model component for catchments not impacted by snow conditions.

GR4J was calibrated for each gauged catchment using the historical precipitation and temperature from Section 2.2 Precipitation generation methodology, maximising the Kling-Gupta efficiency (KGE) score against historical streamflow (Gupta et al., 2009). The Elbe study region here features 59 gauged catchments, each meeting a minimum KGE score of 0.3 for calibration quality: the KGE scores range 0.53–0.88, with 90% between 0.71–0.83 and a median of 0.78.

For catchments without adequate historical streamflow data (either because it is too low in quality, of too short a duration for adequate calibration, or missing entirely), a nearest neighbour calibration approach was used determined by catchment characteristics rather than geographical distance. These characteristics include area, slope, altitude, climate classification (Kottek et al., 2006), land cover classification (Arino et al., 2012), and soil classification (Zobler, 1999), using a Gower weighted distance metric. The calibrated parameter set for the nearest neighbour catchment is used as a surrogate for the ungauged catchment, with weather data aggregated to the ungauged catchment.

The simulated precipitation and temperature from the 1008-member PrecipHENS ensemble was used as input to the calibrated GR4J models to produce daily winter streamflow for each catchment. The initial catchment state in the GR4J model was set by first creating a modelled streamflow time series for the historical period using historical precipitation and temperature and extracting the internal states of the GR4J simulation. For each simulated winter season of weather, a season of river flow was generated from each of internal states on the 1 December (the date at which the winter simulations start) from each of the historical years (1981–2024). The internal states from December 1980 were not used to allow a burn-in period to the GR4J simulation on the historical data. This results in a total river simulation ensemble of 43344 seasons (1008 seasonal weather simulations and 43 GR4J initial conditions).

https://doi.org/10.5194/egusphere-2025-5841
Preprint. Discussion started: 9 December 2025

3 Results

3.1 Precipitation generation results

We first evaluate the precipitation fields generated by the benchmark statistical model and by PrecipHENS against the historical reference data, applying the four criteria (G1–G4) introduced in Section 1.1.3 Precipitation . These criteria assess whether each method reproduces the observed precipitation climatology (G1), spatial and temporal coherence (G2), representation of extremes (G3), and methodological robustness (G4). The subsections below address these in turn.

3.1.1 Preservation of observed climatology

Figure 4 shows the spatial distribution of the mean daily precipitation on wet days (>1 mm) and the number of wet days across the historical dataset, the benchmark simulated dataset, and PrecipHENS dataset. The two simulated datasets reproduce the major climatological features of winter precipitation across the Elbe region shown in the historical data, including increased precipitation in the south-west and lower totals in the north and central basin. The benchmark closely matches the observed spatial gradients and magnitudes, which is the result of the stationary block bootstrap on non-extreme precipitation. PrecipHENS also demonstrates strong agreement with the observed climatology, successfully capturing the large-scale spatial structure and key precipitation gradients across the region. The number of wet days is consistent across all datasets, indicating that both methods realistically simulate precipitation occurrence. A view of the bias between the historical dataset and both the benchmark and PrecipHENS is provided by Figure B1. This shows a dry bias in PrecipHENS in the wettest regions of the domain. However, this bias is small and within 0.5 standard deviations of the historical record. These results demonstrate that both approaches (benchmark and PrecipHENS) preserve the key features of observed winter precipitation climatology (**G1**). PrecipHENS produces additional meteorological variables, including surface temperature as used for hydrological modelling. As such, Figure B2 gives the equivalent Figure 4 and Figure B1 for surface temperature, demonstrating overall that PrecipHENS also preserves the historical winter surface temperature climatology.

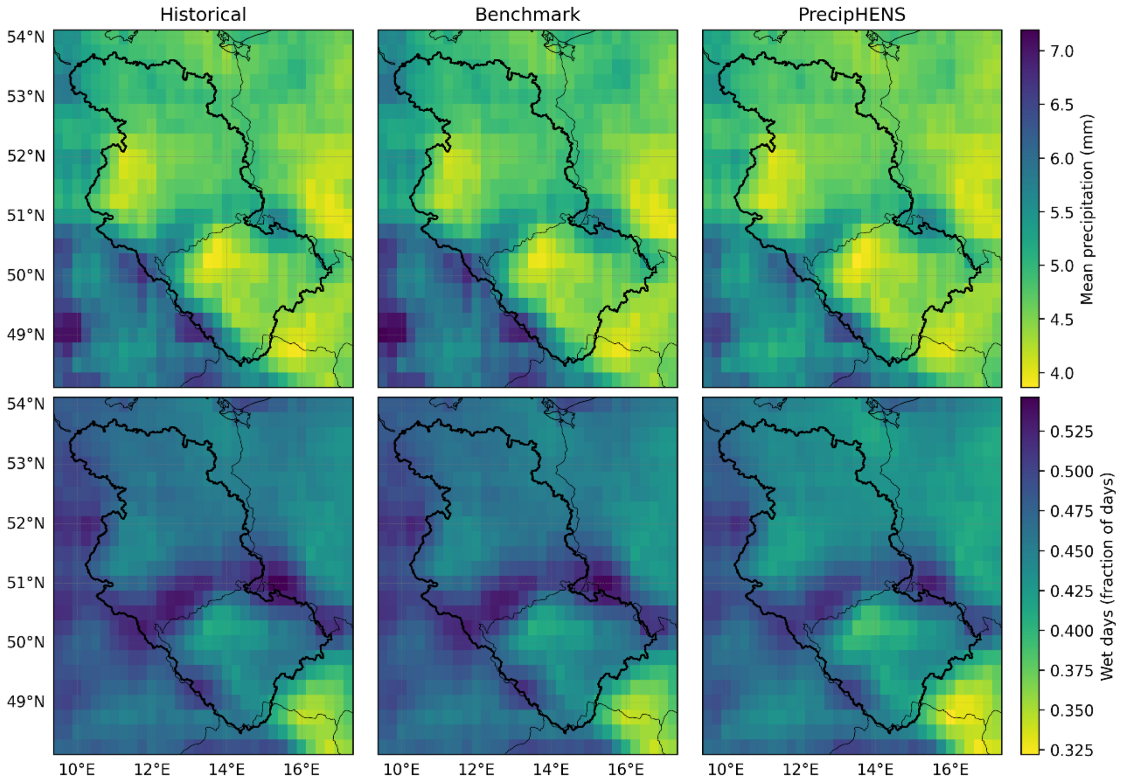

Figure 4: Comparison of mean daily precipitation over wet pixels (>1mm, top row) and the fraction of days with precipitation >1mm (bottom row). In each case data is presented from the historical (left), the benchmark (centre), and PrecipHENS (right).

3.1.2 Realistic spatial and temporal coherence

We assess spatial dependence in daily precipitation through two metrics: the Pearson correlation (r) (Pearson, 1895) and the Ledford–Tawn tail coefficient (η) (Ledford and Tawn, 1996). Pearson's r is a summary of the correlation in the bulk of the precipitation distribution, capturing the spatial organisation of typical precipitation variability. As flood risk is primarily driven by rare and spatially extensive extremes, the correlation specifically in the tails of the precipitation distribution is explored with η. This metric characterises the strength and decay of extremal co-occurrence between pairs of variables (locations, here). Correlation fields of daily precipitation with a single location (Dresden) are shown in Figure 5 and demonstrate that all three datasets – historical, benchmark, and PrecipHENS – exhibit similar spatial gradients and correlation decay. For the tail correlation, the results for η show that the benchmark approach reproduces the large-scale spatial structure of the historical data but also inherits its local variability, due to being constructed directly from a finite sample of past extreme events. In contrast, PrecipHENS yields a smoother spatial field that aligns with the dominant features seen in the historical data but avoids replicating its local sampling noise. Compared to the historical data, this smoother structure arises from the use of a much larger set of diverse, simulated seasons, allowing for more stable estimation of tail dependence patterns across space. In contrast, the typical precipitation correlation represented by Pearson's r has a smooth gradient across all three datasets owing to the larger sampling size, even in the historical record length.

For the tail correlation, Figure 6 extends the single site results presented in Figure 5 to evaluate whether this behaviour holds more generally across the domain, computing η from each location to all other grid points and grouping the results by distance. All three methods exhibit the expected monotonic decay in η with distance, reflecting the weakening spatial dependence of extremes at greater separations. The benchmark and PrecipHENS both closely follow the historical curve, confirming that it reproduces the same underlying extremal structure. The PrecipHENS ensemble displays a narrower uncertainty band compared to the historical and benchmark data, which may indicate the smoothing across events arising from its ability to sample a wide range of plausible events, particularly between locations of higher distances apart that feature fewer joint events in the historical record.

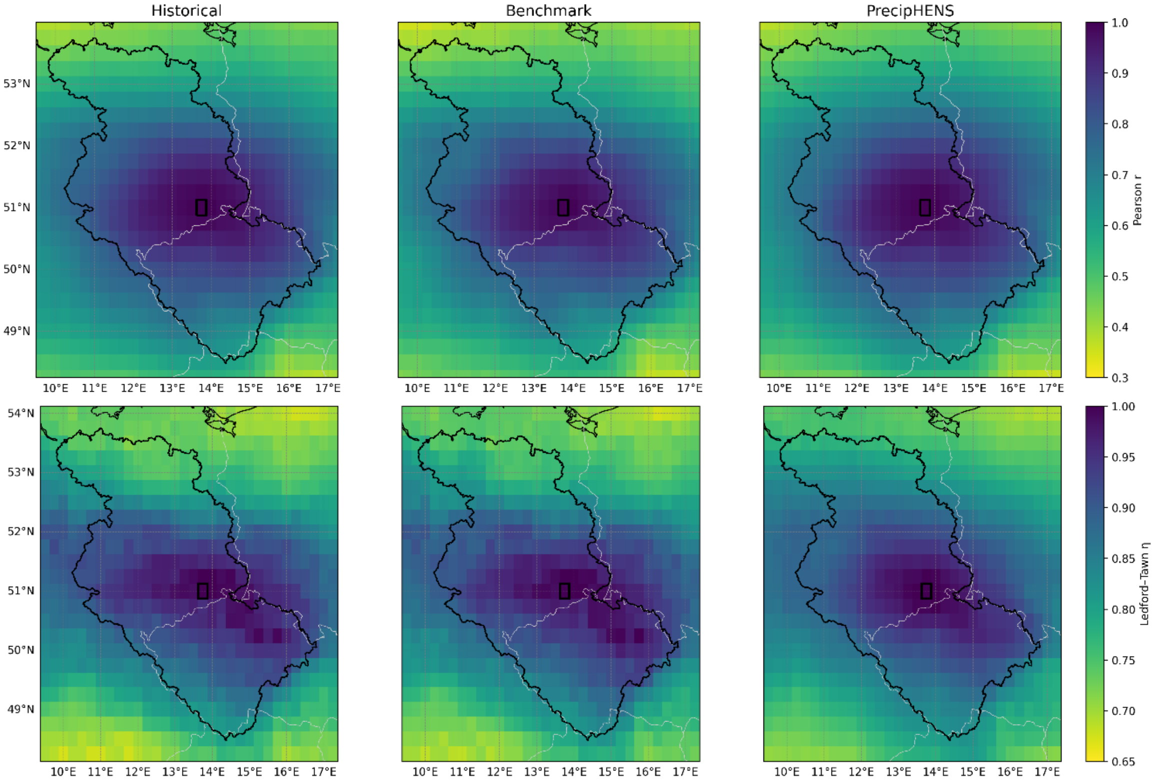

Figure 5: Correlation between daily precipitation at a reference location (Dresden; black square) and all other grid cells, computed across the winter period. Panels show results for historical data (left), benchmark simulations (centre), and PrecipHENS simulations (right). Correlation is shown for all data with Pearson's r (top row) and for extreme correlation with the Ledford–Tawn tail dependence coefficient (η) (bottom row, quantile threshold of 0.9).

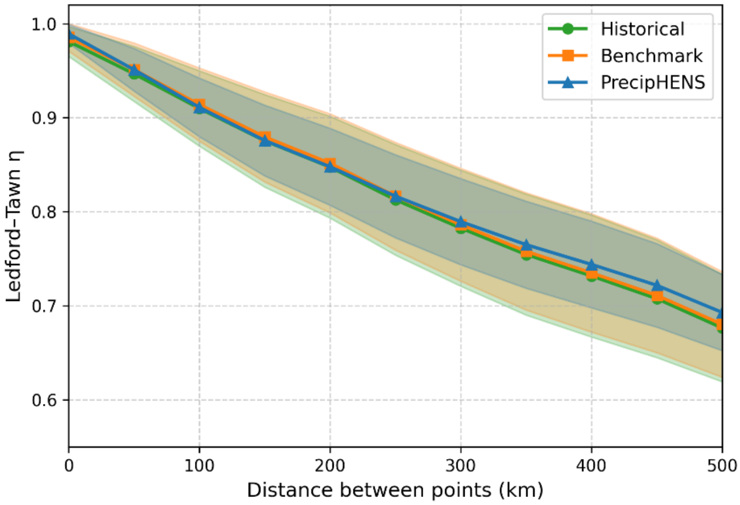

Figure 6: Ledford–Tawn tail dependence coefficient (η) as a function of distance between grid point pairs, computed from all grid points. Curves show historical data (green), the statistical benchmark (orange), and the PrecipHENS ensemble (blue), with shaded bands indicating ±1 standard deviation.

Temporal correlation in precipitation at a location is a key aspect for flood risk estimation because of the importance of compound or prolonged rainfall episodes in determining the ground saturation that impacts river flow. We assess temporal dependence in daily precipitation using the same two metrics as above – Pearson's r and η – each at a lag of 1 day. Pearson's r at lag-1 day provides a summary of linear dependence in the bulk of the precipitation distribution, reflecting how typical wet or dry days relate to conditions on the previous day; η complements this by characterising extremal persistence, measuring the likelihood that large precipitation values occur on consecutive days.

Figure 7 shows maps of these temporal correlation metrics computed at each grid cell for the three datasets. The benchmark and PrecipHENS simulations again broadly reproduce the temporal structure seen in the historical record. PrecipHENS displays smoother spatial variation than the benchmark, but also lower similarity in general across the domain – again, likely a construct of the benchmark being constructed by resampling and perturbation from a finite sample of multi-day historical events. Additional evidence for this comes from inspecting the durations of wet spell events over the season at the example site of Dresden (Figure B3) noting that the noise in the small sample of multi-day wet spells in the historical record drives what is seen in the benchmark data.

These results demonstrate that both approaches (benchmark and PrecipHENS) preserve the key features of observed spatial and temporal coherence, but that PrecipHENS is not sensitive to the limited observed tail variability in the historical record (**G2**). The spatial correlation in the temperature displays a smooth surface across all datasets, like the precipitation example in the top row of Figure 5. We do not include this here for brevity, nor do we include tail temperature correlation because extreme temperature is not the focus of this present study.

https://doi.org/10.5194/egusphere-2025-5841
Preprint. Discussion started: 9 December 2025

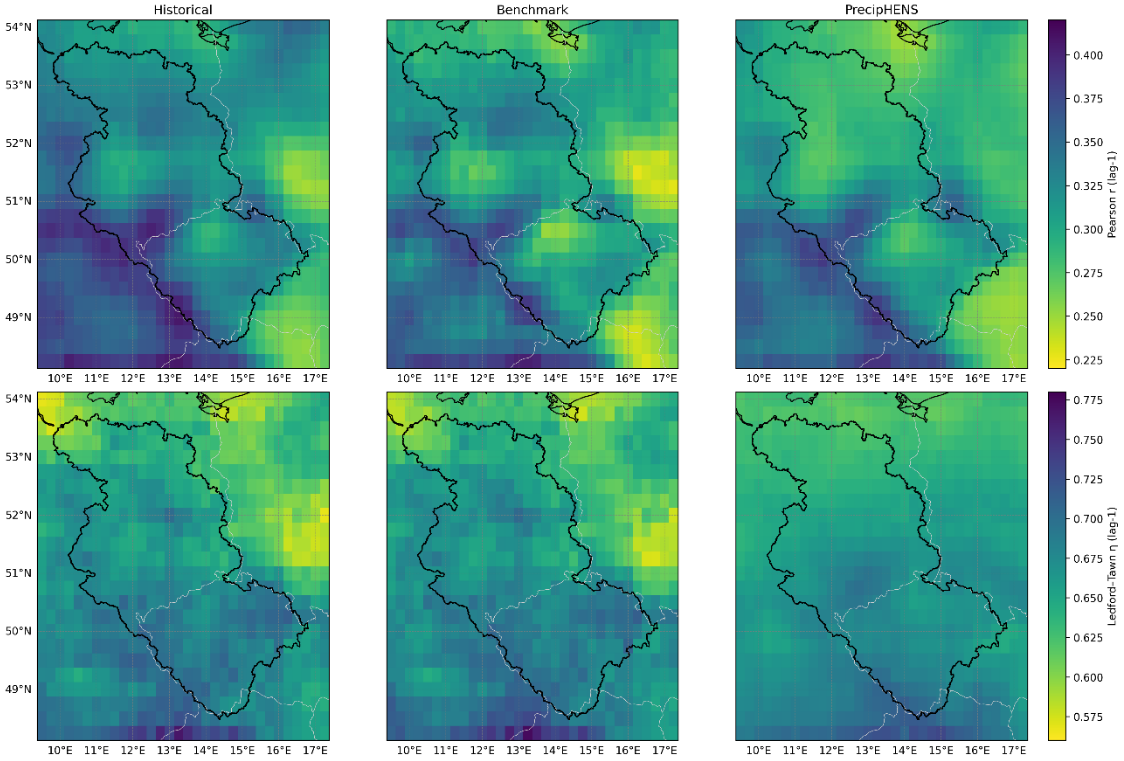

Figure 7: Correlation between daily precipitation at a location and the following day (i.e. 1-day lagged correlation per site), computed across the winter period. Panels show results for the historical data (left), benchmark (centre), and PrecipHENS (right). Correlation is shown for all data with Pearson's correlation (top row) and for extreme correlation with Ledford-Tawn tail dependence coefficient (bottom row, quantile threshold of 0.9).

3.1.3 Realistic extreme event representation

Both the frequency and magnitude of precipitation extremes influence flood risk, so biases in either can distort risk estimations. Having already examined spatial correlation of extremes (e.g. Figure 5), we now assess the marginal behaviour of daily precipitation extremes at each grid cell. Rather than reproducing the historical record – which is too short for reliable tail estimation – we evaluate whether the simulations exhibit plausible distributions and spatial patterns in their extremes. The creation of long stochastic datasets such as the benchmark and PrecipHENS is motivated precisely by this need to explore physically realistic but unobserved extremes.

For each of the historical, benchmark, and PrecipHENS datasets, we compute the seasonal maxima of daily precipitation at each location and fit a Gumbel distribution via maximum likelihood. The Gumbel distribution – a special case of the generalised extreme value (GEV) distribution that fixes the shape parameter – is used here to avoid instability in fitting across locations. The GEV shape parameter can be highly uncertain for short historical records, leading to inconsistent tail behaviour across the region.

https://doi.org/10.5194/egusphere-2025-5841
Preprint. Discussion started: 9 December 2025

The location and scale parameter fits are shown in Figure 8 for each dataset. The spatial patterns in regions of higher Gumbel location parameter (thus higher precipitation extremes) and higher Gumbel scales (thus higher precipitation extreme variability) are similar. However, the benchmark model data displays higher fitted values of both Gumbel parameters than PrecipHENS. The local, marginal Gumbel parameters of the PrecipHENS simulations are closer to those of the historical data than are the benchmark model's, even though the benchmark model is based on inference about the extremes, whereas the PrecipHENS is a more general model. There is a generally coherent, smooth spatial structure in the tail distributional fits across the region, which, although fit independently per site, is consistent with the evidence of Figure 5 that there is high spatial correlation in the extreme precipitation.

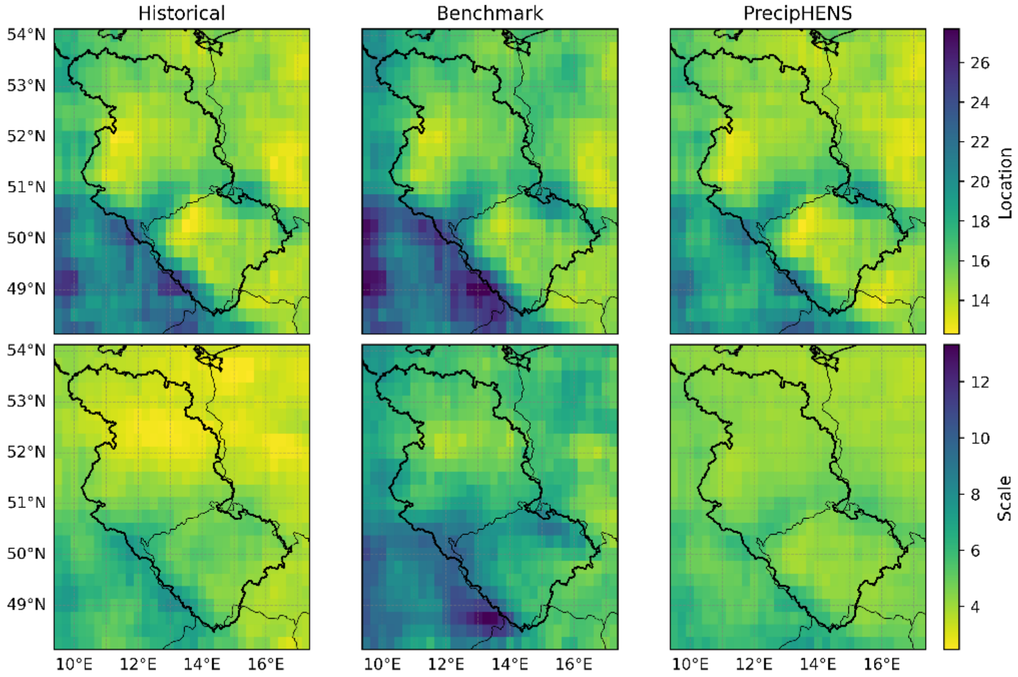

Figure 8: Extreme marginal distributional fit for 1-day precipitation, based on a Gumbel distribution fit to winter maxima. The location (top) and scale (bottom) parameters are shown for the historical period (left), benchmark (centre) and PrecipHENS (right).

To understand the joint contribution of the two parameters in the Gumbel fits, Figure 9 gives the return level for precipitation for a range of return periods (2, 5, 10, 20, 100 years) at each site across the region, comparing this level under the model fitted to the historical data and the benchmark or PrecipHENS, respectively. A perfect agreement between historical and simulated fit is given by the dashed line for reference, and although it is not expected that (or an aim for) the data sit on this line, there is an expectation for a spread around the agreement line that increases with the return period and the associated uncertainty in estimation of such a return level with the limited historical data record. For example, the 2-year return level should be well estimated by the historical data (being 44 years in length) and we therefore expect there to be strong agreement between the simulated and historical data, whereas the 100-year return level is not well estimable from the historical data and is expected to have high spread.

In addition to the 1-day precipitation model results from Figure 8, GEV models are fit to longer accumulations of 3- and 10-days, to explore the temporal structure of the extremes. Figure 9 suggests that the benchmark approach tends to over-represent the tail of precipitation, and that this over-representation accelerates as the tail becomes more extreme. This is likely due to the methodology of the statistical extrapolation, whereby the historical events are repeated and perturbed at the rate of the limited historical record, without consideration of whether the representation in the historical record is uniformly likely. For example, the method is sensitive to the presence of a rare, extreme event that is in the historical input record and is likely over-sampling the rarest, most extreme observed events. The return levels of PrecipHENS are more in agreement with the historical data at low return periods (2–10 years) than the benchmark method and are distributed around the agreement line at the higher return periods (20–100 years). Compared to the historical data, the variability from the historical distributional fits for the PrecipHENS data at high return periods tends to show that the return level is inflated for sites with lower extreme precipitation magnitudes and deflated for sites with higher extreme precipitation magnitudes.

The marginal tail distribution results presented here suggest that the PrecipHENS data features extreme precipitation at an acceptable frequency and magnitude (G3): it is similar to the historical data and improves upon a likely over-sampling of repeated extremes in the benchmark approach, which occurs when it is built on a limited record of historical input data. This is a promising result for the AI-powered weather generation, which has previously been critiqued for a lack in ability to generate extremes (Mahesh et al., 2024b), albeit the analysis here is conducted on aggregated values and not the 6-hourly temporal resolution the SFNO model outputs. The joint tail distribution across sites has been explored in the correlation discussion of the previous section, and we also explore the distribution of precipitation events as high-dimensional spatiotemporal clusters in the next section, showing that PrecipHENS has a smooth extrapolation from the historical examples of precipitation storm features (see Figure 10).

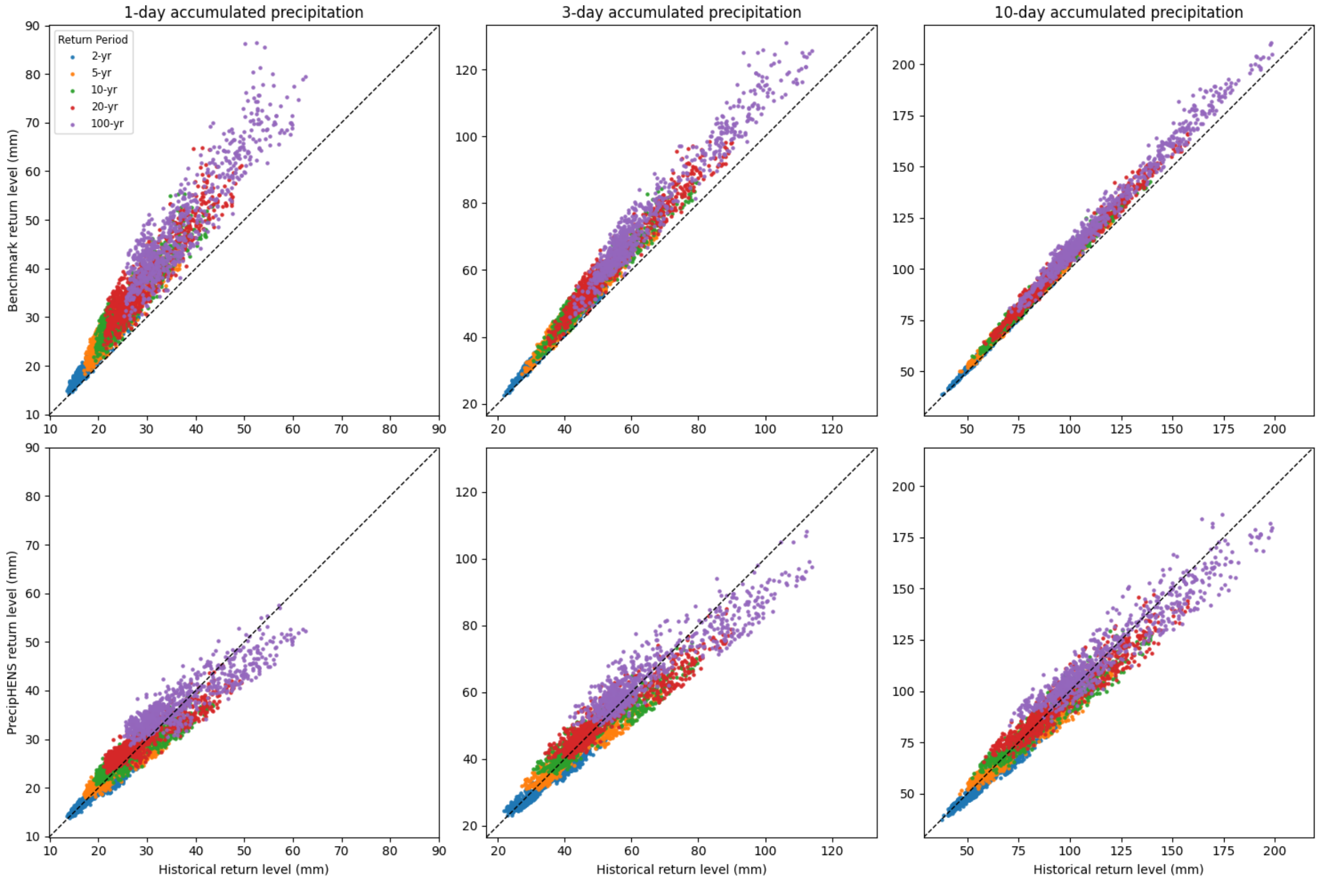

Figure 9: Comparison of modelled (benchmark in top row, PrecipHENS in bottom row) and historical precipitation return levels for a range of return periods (2, 5, 10, 20, 100 years) and durations (1-day, 3-day, 10-day). Each dot represents a single grid point. The different return periods are differentiated by the colours. The black 1:1 line indicates perfect agreement between modelled and historical return levels. Return levels are estimated using Gumbel fits to each respective dataset, for example in the case of the 1-day accumulated precipitation (left-most column), this is the Gumbel fit shown in Figure 8.

3.1.4 Methodological robustness and generalisability

Statistical models for weather generation, such as the Heffernan and Tawn (2004) framework, are inherently tied to historical data since they construct multivariate relationships based on observations. While these approaches effectively capture statistical extremes within the historical record, they are fundamentally limited by the length and completeness of the observational dataset. As a result, they are constrained in their ability to produce new and unseen weather events. In contrast, AI models such as SFNO are designed to learn a latent representation of the underlying dynamics and interactions between meteorological variables. SFNO captures the spatial and temporal dependencies across the full atmospheric system, allowing it to generalise beyond the direct constraints of historical data (Bonev et al., 2023). Furthermore, SFNO-powered ensembles, such as the HENS approach have shown that these ensembles can produce plausible, yet novel extremes (Mahesh et al., 2024b).

To compare the structural variability in extreme precipitation across the historical, benchmark, and PrecipHENS datasets, we perform a principal component analysis (PCA) on grid-point-level precipitation fields. The PCA is fitted to the historical data, for days which have a precipitation value exceeding the 90th percentile threshold for that grid point. This analysis provides insight into the dominant modes of variability in the historical extreme precipitation days, helping assess whether the different precipitation generation methods generate variable weather patterns and – because the PCA is fit only to historical data – how this extrapolation in the simulated data relates to the structure in the historical data.

Figure 10 compares the first two principal components (PC1 and PC2), with points coloured by dataset. These two components account for 67.8% of the total variance in the historical extreme precipitation data (46.5% and 21.3% for PC1 and PC2, respectively), offering meaningful low-dimensional representation. Many of the benchmark points follow distinct vectors originating from near the origin. These vectors reflect the constrained modes of variability tied closely to the historical data used to construct the benchmark. The increased severity of extremes in the benchmark dataset (as shown in Section 3.1.3 Realistic extreme event representation) is reflected with the points extending further from the origin than in the other two datasets. In contrast, PrecipHENS produces a more continuous spread of points, introducing a wider distribution of precipitation patterns whilst also extrapolating beyond the historical data.

To quantify how broadly each dataset captures this PCA space, we compute the proportion of non-overlapping 1×1 grid cells in PCA space that contain at least one event from each model. PrecipHENS spans 80.9% of these cells, compared to 50.1% for the benchmark and 18.8% for the historical record. This reinforces the conclusion that PrecipHENS generates a broader diversity of extremes than the other methods.

The starred point in Figure 10 is the most extreme day in the historical record at Dresden, defined here as the day with the highest 1-day precipitation in the grid cell over the centre of Dresden (30 December 2003). Figure 11 shows the spatial precipitation pattern associated with the event. The event serves as a meaningful anchor in PCA space against which simulated extremes can be compared. To assess how each method reproduces physically plausible yet varied extremes, Figure 12 shows the precipitation patterns for the eight nearest events in PCA space for the benchmark and PrecipHENS. All 16 events – i.e., eight events from both datasets – are close in PCA space, reflecting broadly similar storm structures across methods. However, clear differences emerge in the diversity of spatial precipitation patterns.

The benchmark method events display limited variability, with similar spatial footprints and precipitation concentrated in nearly identical regions across panels for six of the eight events, matching that of the historic event in Figure 11. This repetition reflects the structural constraint of the statistical benchmark model, which, despite reproducing extreme values, tends to repeat historical spatial configurations with minimal deviation.

In contrast, the PrecipHENS events exhibit a broader range of spatial characteristics. While the overall structure of the storms remains similar (as expected given their PCA proximity to the historical reference), there is more noticeable variation in the location of precipitation maxima, the extent of wet areas, and the storm footprint shape. This highlights the SFNO model's ability to produce diverse and novel patterns, even when constrained to closely match a known historical extreme, supporting the model’s potential to simulate a wider range of realistic high-impact events (**G4**).

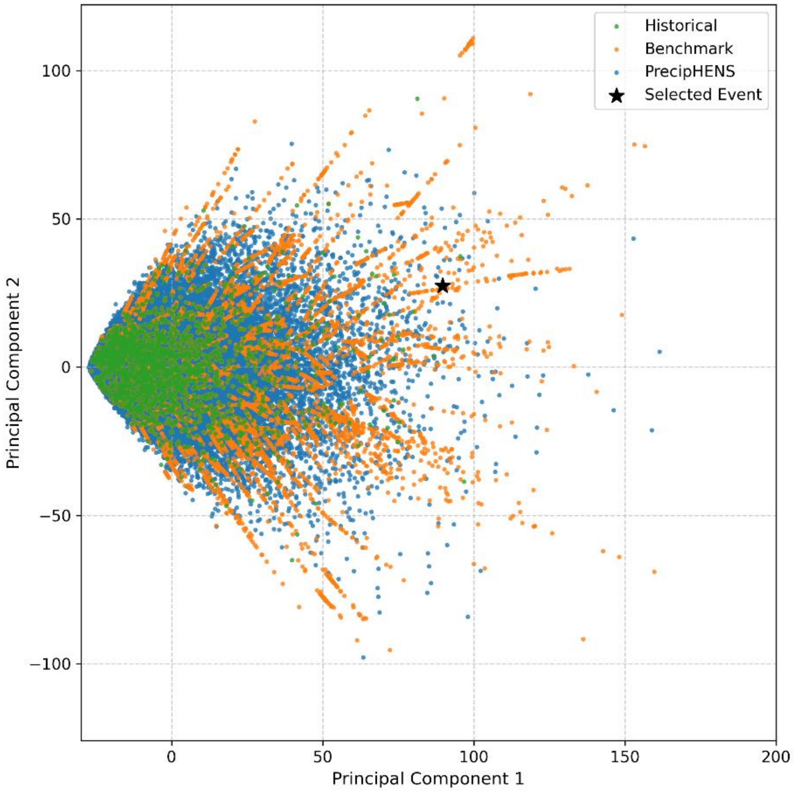

475 **Figure 10: Principal component analysis (PCA) of daily extreme precipitation fields from the Historic, Benchmark, and PrecipHENS datasets. Each point represents a single extreme day projected onto the first two principal components (PC1 and PC2), summarising the dominant spatial variability in precipitation patterns. The starred point indicates the highlighted observed event (30 December 2003), shown in Figure 11.**

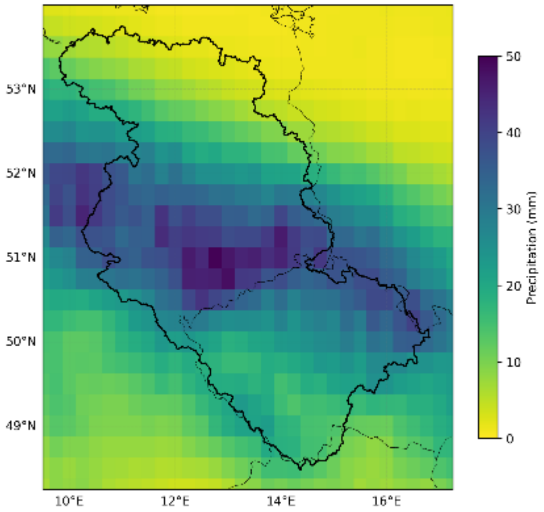

480 **Figure 11: The precipitation pattern of the starred event in Figure 10, representing the most extreme observed event impacting Dresden, based on the maximum 1-day precipitation over the grid cell covering central Dresden.**

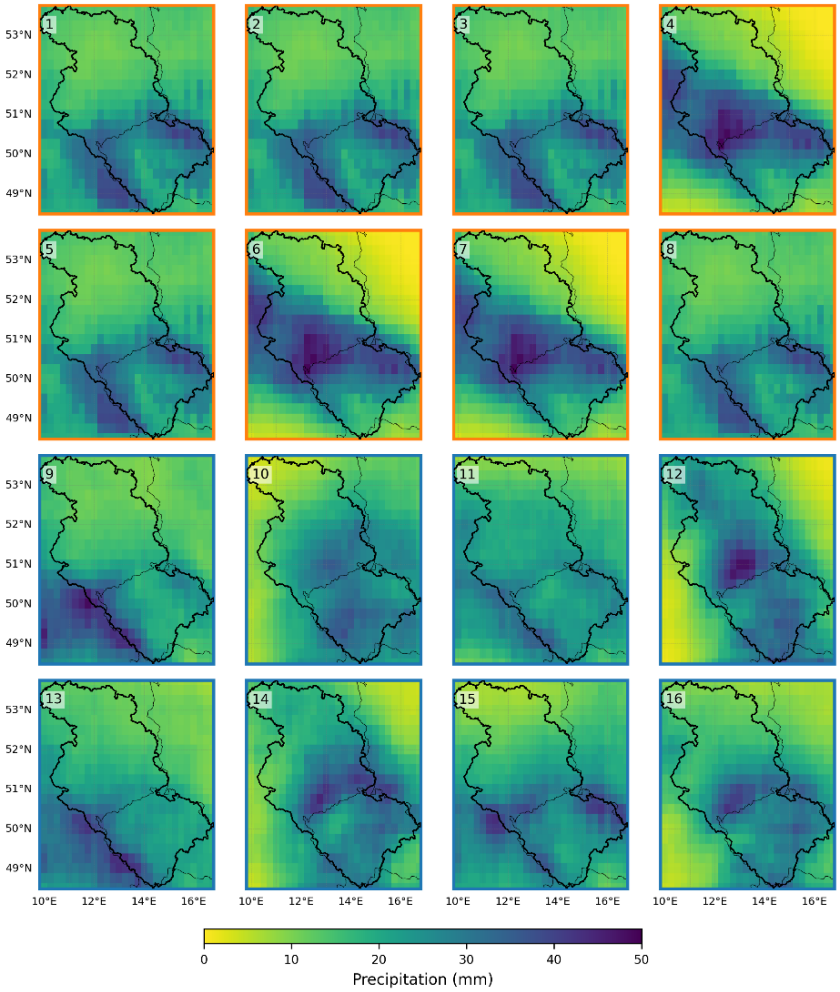

Figure 12: Precipitation fields corresponding to the eight simulated events that are closest in PCA space to the historical reference event, drawn, respectively, from the benchmark model (plots 1–8, top two rows with orange outline) and from PrecipHENS (plots 9–16, bottom two rows with blue outline).

3.2 River flow generation results

This section describes the use of the simulated weather from the 1008-member winter seasonal ensemble of PrecipHENS as input to a hydrological model, along with initial catchment conditions from the modelled historical period. The four goals from Section 1.1.3 Precipitation related to estimation of tail risk are revisited in relation to the simulated river flow as a dataset for flood risk estimation.

3.2.1 Preservation of observed climatology

Figure 13 shows the spatial distribution of mean river flow for large catchments (> 2500 km^2) in the historical and PrecipHENS datasets, alongside the standardised bias between them. The historical climatology is calculated as the average of the 43 seasons of historical flow, whereas the PrecipHENS climatology is the average of 1000 bootstrapped samples, each of which is a sample of 43 seasonal simulations from the 1008-member ensemble combined with the historical sequence of initial catchment conditions. The bootstrap sampling design used here is to ensure a fair comparison of the bias in weather-driven flows as opposed to initial seasonal conditions, with each 43-member bootstrap sample from PrecipHENS including one ensemble member aligned with each of the 43 historical initial conditions. The PrecipHENS simulations closely reproduce the observed large-scale patterns in the historical data, with peak flows in the central and downstream regions and weaker flows in the south, east and west. The bias of PrecipHENS versus the historical data (Figure 13, right) is small and consistently negative, falling within a modest range below one standard deviation of the historical data.

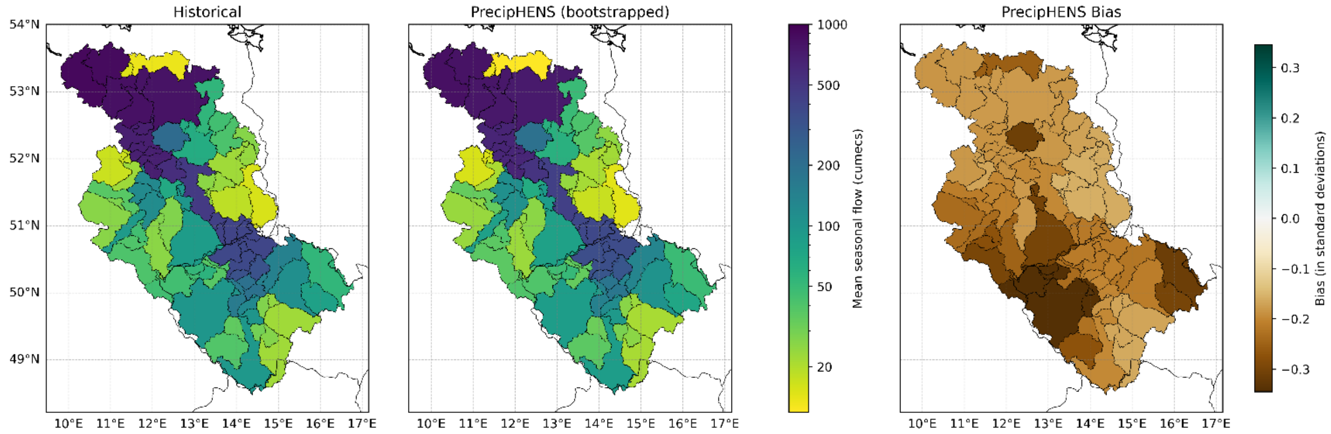

Figure 13: The average winter seasonal flow, shown only for catchments in the Elbe with area above 2500km^2 (all catchments are shown in a version in Figure C1). The historical (left) and PrecipHENS (middle) seasonal means are shown, along with the bias between these (PrecipHENS minus historical), standardised by the standard deviation in the historical seasonal mean (right).

Figure C1 shows the results highlighted in Figure 13 but for all catchments across the Elbe basin. This confirms that the agreement between historical and PrecipHENS average flows extends across all catchments in the domain, not just the largest. The spatial structure and magnitude of mean river flows are consistently well reproduced, and the observed negative bias is modest and spatially coherent. While this points to a small dry tendency in the simulations, it is not large enough to affect the overall climatological fidelity and is not unexpected given that there was found to be a small dry tendency in the precipitation and a small warm tendency in the temperature (Figure B1, Figure B2). Together, these results confirm that PrecipHENS-driven simulations capture the key features of observed winter river flow climatology (**G1**).

https://doi.org/10.5194/egusphere-2025-5841
Preprint. Discussion started: 9 December 2025

3.2.2 Realistic spatial and temporal coherence

As in Section 3.1.2 Realistic spatial and temporal coherence, we assess the spatial and temporal coherence of simulated river flows by comparing correlation patterns across the domain, using both Pearson's correlation coefficient (r) and the Ledford–Tawn tail dependence coefficient (η) to give a quantifiable measure of correlation across the basin in space and time. We also include an anecdotal example of river flow across the winter season and along the main trunk of the Elbe to illustrate the high temporal and spatial correlation that is generally present in river flow data (see Figure C2 for a visualisation of this).

Figure 14 shows time series of flow across the main Elbe trunk during a single example season from each of the historical and PrecipHENS datasets. It is important to note that these are two independent seasons, and so the goal here is not to compare them as like for like flow simulations that aim to match one another. From this example, the timing and progression of peaks clearly illustrate the propagation of flow through the river network, with PrecipHENS capturing upstream to downstream temporal evolution and magnitude increase in the flow.

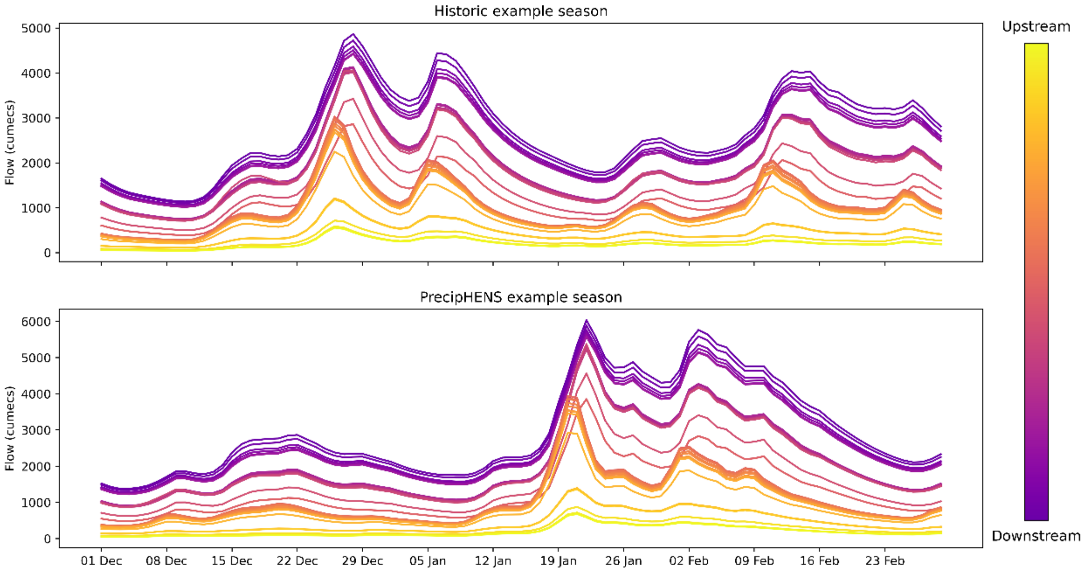
Historic example season

PrecipHENS example season

Figure 14: An example of hydrologically modelled river flow for an example historical season (top) and simulated PrecipHENS season (bottom) across the 30 catchments that form the main trunk of the river Elbe. See Figure C2 for a map of this set of catchments.

Figure 15 shows spatial correlation patterns for the Dresden reference catchment, comparing PrecipHENS against the historical data. PrecipHENS captures the dominant spatial structure of flow seen in the historical record, including strong upstream-downstream coherence along the Elbe and weaker correlations across sub-basins. Unlike the precipitation correlation, which is expected to be a relatively smooth spatial field, the expected correlation in river flow between catchments will largely rely on three factors: the upstream-downstream network structure; the proximity between catchments, which influences their shared exposure to weather patterns; and the relative size of the contributing areas, with large upstream catchments exerting a stronger influence on downstream flow than smaller ones. This final point is illustrated in Figure 15: several catchments south-east of Dresden show stronger correlations with the Dresden site, consistent with their higher average flows, as shown in Figure 13.

While Pearson's r fields are closely matched in Figure 15, the extremal correlations in PrecipHENS, represented by η, are generally higher than in the historical data, indicating modestly stronger extremal dependence. These differences likely reflect the larger ensemble size and richer sampling of extremes in PrecipHENS, which yields smoother and more stable estimates of extremal dependence compared with the more variable historical data, rather than any systematic bias. This behaviour is consistent with the precipitation results, where the noisy spatial pattern of η in the historical data is comparably smoother in the larger PrecipHENS ensemble.

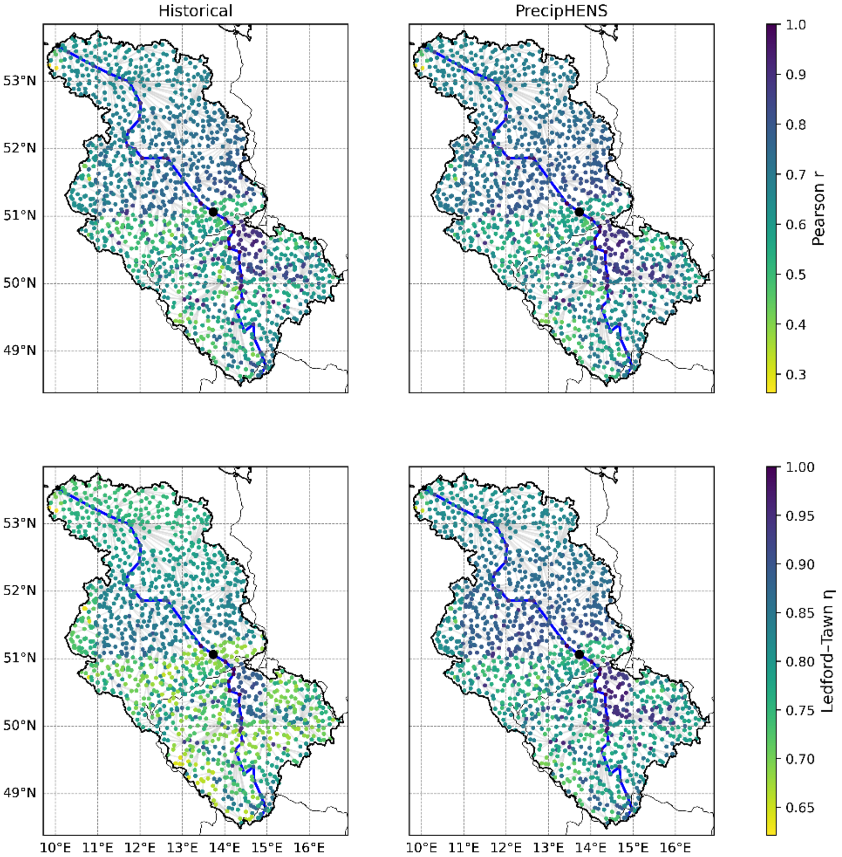

Figure 15: Correlation between daily river flow at a reference location (Dresden; black circle) and all other river catchments, computed across the winter period. In each case, only the outflow point of the catchment is shown as a point, and the grey connections highlight the structure of the river network, with the main trunk of the Elbe highlighted in the blue line. Panels show results for historical data (left) and PrecipHENS simulations (right). Correlation is shown for all data with Pearson's r (top row) and for extreme correlation with the Ledford–Tawn tail dependence coefficient (η) (bottom row, quantile threshold of 0.9).

This temporal correlation at a single day lag is given in Figure 16 (and at a 10-day lag in Figure C3). The 1-day and 10-day lagged Pearson's r and η values across the basin are comparable between PrecipHENS and the historical data. At a 1-day lag, the correlation – generally and in the extremes – is high across the region (lowest Pearson's r being above 0.7). This is particularly so in the northern region of the Elbe, explaining the clear separation between slow-responding catchments in the lowlands and fast-responding catchments in the more mountainous southern region. This demonstrates that PrecipHENS precipitation, when fed through the GR4J hydrological models, induces the strong autocorrelation expected in streamflow even without explicit river flow routing between the modelled catchments.

The anecdotal and quantitative examples presented here suggest that PrecipHENS preserves the spatial and temporal coherence of observed river flows across the Elbe network in comparison to the historical modelled data (**G2**).

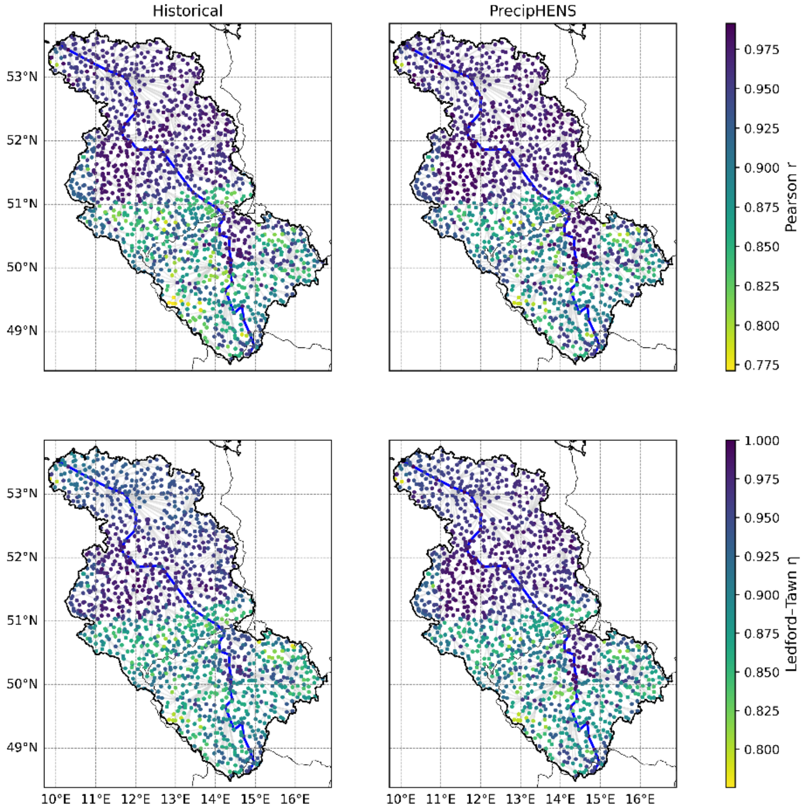

Figure 16: Correlation between daily river flow at each catchment and the flow at that respective catchment the following day (i.e. lag of 1 day), computed across the winter period. In each case, only the outflow point of the catchment is shown as a point, and the grey connections highlight the structure of the river network, with the main trunk of the Elbe highlighted in the blue line. Panels show results for historical data (left) and PrecipHENS simulations (right). Correlation is shown for all data with Pearson's *r* (top row) and for extreme correlation with the Ledford–Tawn tail dependence coefficient (*η*) (bottom row, quantile threshold of 0.9).

3.2.3 Realistic extreme event representation

Given the strong dependence of river flow extremes on precipitation input, and the established realism of precipitation extremes in Section 3.1.3 Realistic extreme event representation, we expect PrecipHENS to also produce plausible hydrological extremes – provided the temporal sequencing of rainfall is well represented. As shown in Section 3.2.2 Realistic spatial and temporal coherence, the temporal structure of precipitation and resulting flow is preserved, supporting this assumption.

To assess the marginal behaviour of flow extremes directly, we compute Gumbel fits to the seasonal maxima of daily streamflow at each catchment and compare the resulting location and scale parameters between the historical and PrecipHENS datasets. Figure 17 shows strong agreement in both parameters across the larger catchments, with PrecipHENS replicating the spatial structure of flow extremes seen in the historical record. These results support the conclusion that PrecipHENS produces realistic hydrological extremes across the basin (**G3**).

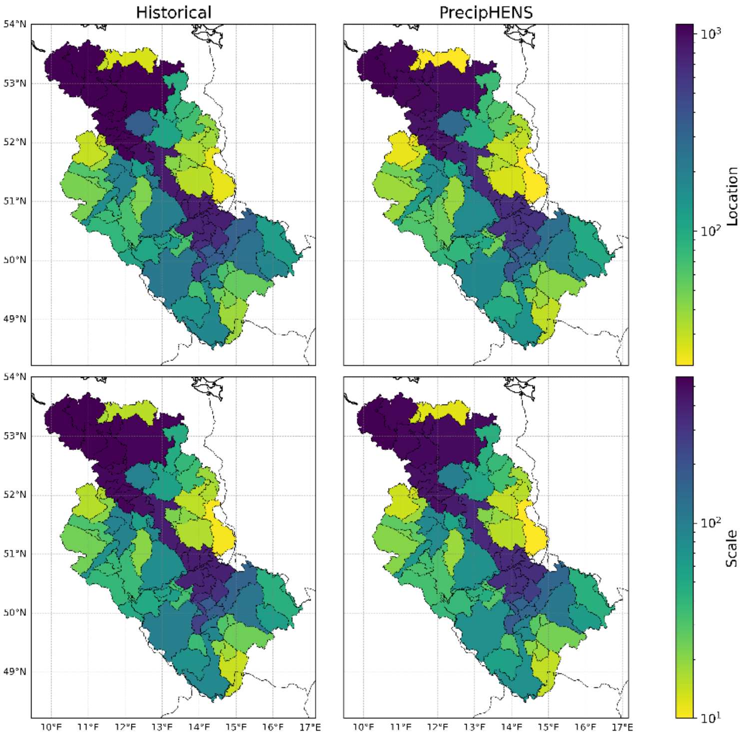

Figure 17: Extreme marginal distributional fit for daily river flow (in cumecs), based on a Gumbel distribution fit to winter maxima. The location (top) and scale (bottom) parameters are shown for the historical (left) and PrecipHENS (right).

3.2.4 Methodological robustness and generalisability

Section 3.1.4 Methodological robustness and generalisability demonstrated that PrecipHENS produces a wide range of plausible yet structurally diverse extreme precipitation events, extending beyond the variability present in the historical or benchmark datasets. Figure 10 showed that PrecipHENS explores a broader region of the PCA space of extreme precipitation patterns, and Figure 12 illustrated that these extremes differ meaningfully in spatial footprint and intensity, even when constrained to be close to a known historical event. Here, we evaluate the hydrological impact of these novel events.

Figure 17 shows the river flow simulations at Dresden resulting from the eight nearest PrecipHENS events (in PCA space) relative to the historic 30 December 2003 storm. Each of these simulations is driven by a precipitation pattern that is distinct from the observed event but similar in overall structure (as shown in Figure 18). The resulting flow responses from each of the storms demonstrate the hydrological variability that PrecipHENS can produce from similar looking events.

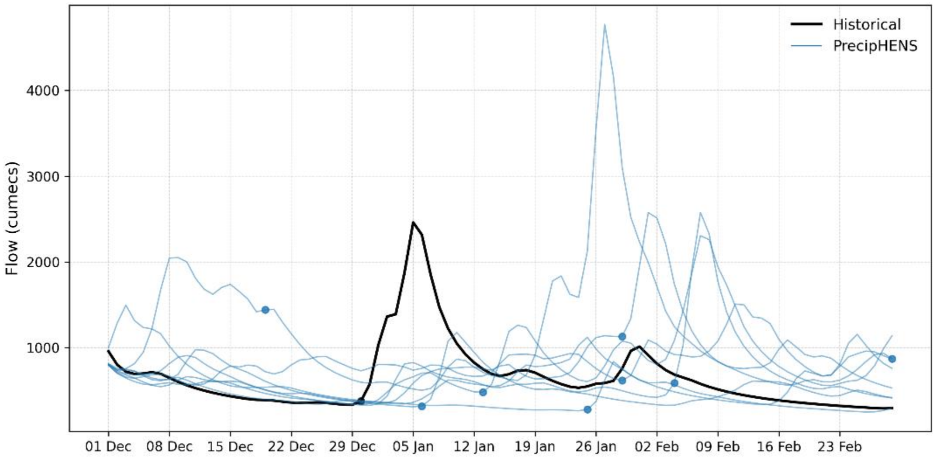

Figure 18: River flow at the Dresden reference location resulting from the eight PrecipHENS ensemble members closest in PCA space to the most extreme observed precipitation event (30 December 2003). Each line shows one season of flow simulation, driven by a distinct AI-generated precipitation pattern, with the blue point representing the time of the selected event. The black line shows the corresponding historical season.

To contextualise these results, Figure C4 compares the full range of river flows simulated from the 43 historical precipitation seasons to the 1008 PrecipHENS simulations driven by a variety of initial catchment states. This wider ensemble view highlights the increased variability introduced by PrecipHENS. The frequency, severity, and timing of flow peaks differ noticeably from the historical record, offering a more diverse and expansive representation of extreme river flow risk. These results show that the methodological robustness and generalisability of PrecipHENS extend beyond atmospheric realism to hydrological impacts (**G4**).

4 Discussion and conclusion

This study introduces PrecipHENS, an AI-powered weather model designed to generate seasonal-scale synthetic weather ensembles for use in flood risk assessment and related extremes analysis. PrecipHENS combines the huge ensembles (HENS) framework based on the Spherical Fourier Neural Operator (SFNO) with the Precipitation AFNO diagnostic precipitation prediction model (Bonev et al., 2023; Mahesh et al., 2024a; Pathak et al., 2022). By evaluating PrecipHENS against an established statistical benchmark – based on the conditional multivariate extreme-value model of Heffernan and Tawn (2004)

– we demonstrate that AI-based weather generation provides a viable alternative for applications such as flood risk assessment and catastrophe modelling at 0.25° resolution.

PrecipHENS meets our four goals outlined in Section 1.1.3 Precipitation : reproducing observed climatology (G1), realistic space–time coherence (G2), and credible extreme behaviour (G3) while maintaining methodological robustness (G4). Unlike traditional statistical models that perturb and extrapolate the historical record, PrecipHENS can generate new, physically consistent weather events that extend beyond observations – an essential capability for representing low-likelihood, high-impact events. When aggregated to the catchment scale, the resulting precipitation and temperature fields drive hydrological simulations that yield realistic river flow responses, confirming the model's suitability for flood risk assessment. Other frameworks also pursue this goal, such as the UNSEEN (Unprecedented Simulated Extremes using ENsembles) approach (Thompson et al., 2017; Kay et al., 2024), which pools large dynamical forecast ensembles to expand the plausible space of extremes. Unlike UNSEEN, which relies on computationally intensive physical forecast models, PrecipHENS achieves a similar outcome through efficient AI-based emulation, offering a flexible and cost-effective alternative.

Despite these strengths, several areas warrant further development. The hydrological modelling in this study assumed initial river conditions derived from an equal resampling of the 44 years of historical input data. A more sophisticated initialisation that captures the full range of seasonal variability and antecedent hydrological states could enhance the realism and variability of simulated flows. Scaling PrecipHENS to continental domains and extending simulations to year-round conditions would broaden its utility, particularly for catastrophe modelling where understanding risk across years and for continental-scale portfolios is essential. Remaining uncertainties concern how well the underlying SFNO emulator reproduces large-scale atmospheric circulation patterns and teleconnections such as the North Atlantic Oscillation (NAO) and El Niño-Southern Oscillation (ENSO), which influence seasonal precipitation patterns. Climatological diagnostics also suggest some under sampling of longer-term variability (Figure 4), indicating a need for further evaluation of how historical variability is represented in PrecipHENS.

Integrating AI-powered weather generation into flood risk assessment has important implications for both research and practice. The ability of PrecipHENS to produce realistic, long-lead seasonal sequences enables generation of stochastic event sets that include plausible yet previously unobserved extremes. This opens opportunities to couple AI-generated meteorology with seasonal forecasts or storyline approaches (Shepherd et al., 2018), providing novel event sequences for stress testing and adaptation planning. The study outlines a practical framework for embedding AI weather emulators into the risk estimation workflows, showing that while AI models need not be developed in-house, effective use will depend on establishing interfaces between model developers and end users. Such collaboration will help tailor outputs for specific hydrological and risk applications and ensure that AI-driven weather generators evolve in ways that meet sectoral needs.

This work represents an initial but significant step toward integrating AI-powered weather simulations into flood risk estimation and catastrophe modelling. Demonstrating the feasibility of PrecipHENS for seasonal-scale weather ensembles and hydrological modelling provides a foundation for extending AI methods to larger domains and longer timescales. As AI weather models continue to advance, their inclusion in probabilistic risk frameworks will become increasingly valuable, offering new opportunities to characterise and manage flood risk in a changing climate.

Appendix A: Data sources for river catchment attributes

The dataset of 68 gauged and 1294 ungauged catchments (shown in Figure 1) within the Elbe River basin modelled within this analysis were associated with a range of attributes to facilitate the modelling of the ungauged basins. This information was extracted from several global-scale datasets as described in Table A1.

Table A1: Catchment attribute data source.

Attribute	Reference
Köppen-Geiger climate classification scheme	(Kottek et al., 2006)
Land use	(Arino et al., 2012)
Soil type	(Zobler, 1999)
Elevation and slope – the 10th, 50th and 90th percentiles per catchment	NOAA global land 1km base elevation
Monthly mean precipitation (1970-2000)	WorldClim (Hijmans et al., 2005)

Appendix B: Additional precipitation results

To extend the precipitation climatology in Figure 4, a bootstrapped sample was performed with each sample being of the same length as the historical record (44 years) and taking 1000 bootstrapped samples. The bootstrapped mean is shown in Figure B1, along with the deviation from the historical climatology. PrecipHENS shows a drier climatology than the historical data, but the difference is within 0.5 standard deviations of the historical mean, indicating that it lies well within the range of typical interannual variability rather than representing a significant bias. PrecipHENS also provides temperature in addition to precipitation, and so a view of the temperature climatology is shown in Figure B2 in comparison with the historical data. As above, a bootstrapped sample was taken to compare. The bias shows a warmer climatology compared to the historical but is again within 0.5 standard deviations from the historical record.

Correlation in time is further explored to the 1-day lagged example in Figure 7 by exploring in more detail the correlation at a single site. Figure B3 gives the distribution of wet day durations at the Dresden example site (where a wet day is defined as a day with >1 mm precipitation). In Figure 7 the correlation is highlighted as being generally lower in PrecipHENS than the benchmark and historical data, and Figure B3 demonstrates that this is due to a higher proportion of single wet day events in the PrecipHENS data in comparison with the historical and benchmark data. In contrast there is a discontinuity in the historical and benchmark data at wet spell durations of 5 days, indicating again that noise in the short historical record drives the benchmark results.

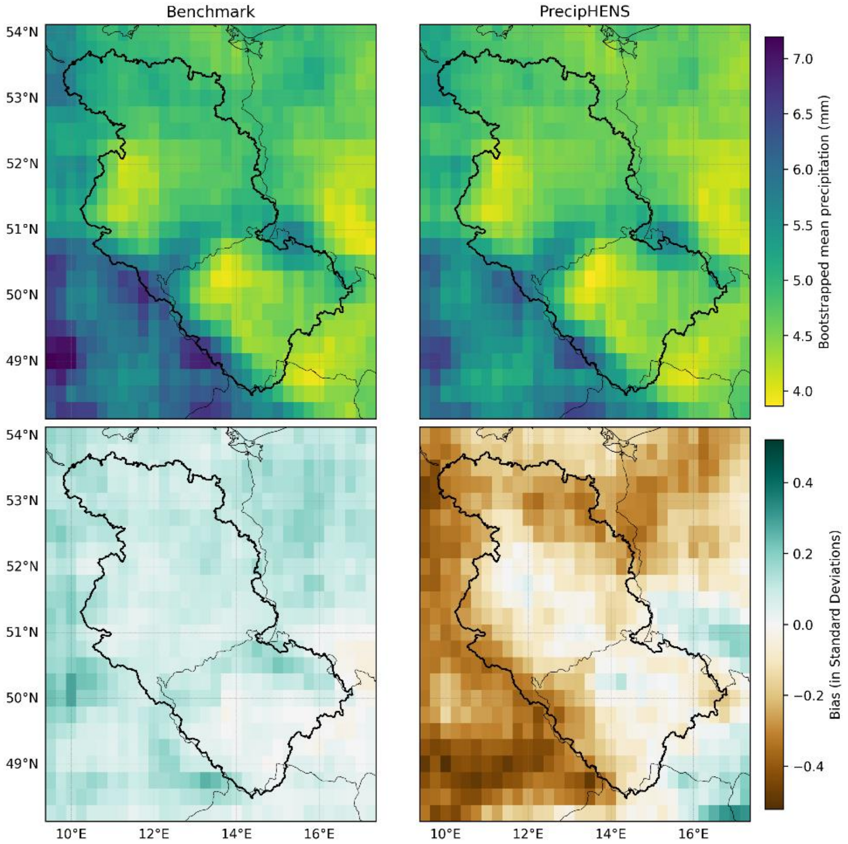

Figure B1: Comparison of mean daily precipitation over wet pixels (>1 mm) as a bootstrapped sample (each sample being of the same length as the historical record (44 years) and taking 1000 bootstrapped samples, top row) and the bias compared to the historical climatology (bottom row). Data is presented from the benchmark (left) and PrecipHENS (right).

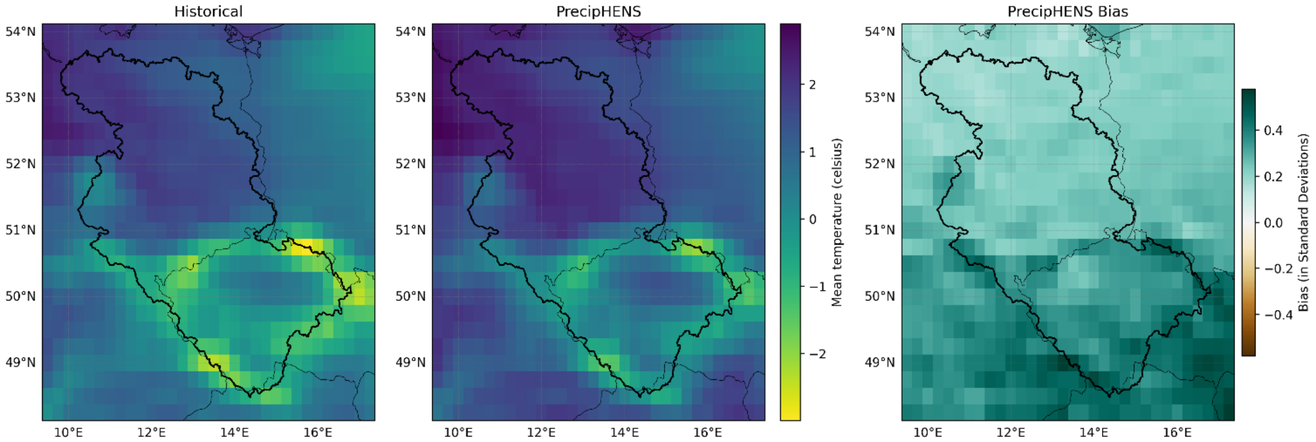

665 **Figure B2: Comparison of mean daily surface temperature in the historical (left) and PrecipHENS (centre). The PrecipHENS data is presented here as the mean of a bootstrapped sample, and the bias from the historical is also shown (right).**

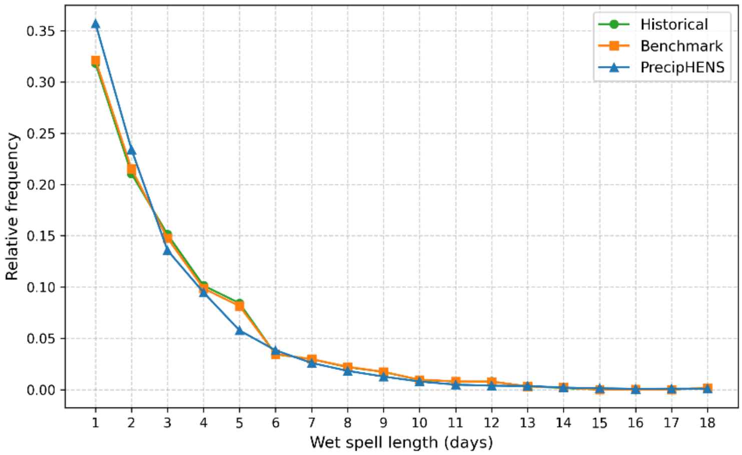

Figure B3: The proportion of multi-day precipitation across the historical, benchmark and PrecipHENS data for the Dresden location. A wet spell is defined as that with more than 1mm daily precipitation, and wet spell duration is calculated as the number of consecutive days above this threshold. The data here is presented as the relative frequency of wet spell durations across those identified at the location.

Appendix C: Additional river results

Additional examples of river results are included to support those presented in Section 3.2 River flow generation results. The climatological river flow across the basin is extended to all catchments in Figure C1 to support the version focusing only on large catchments in Figure 13. This shows that in addition to the average flow being well represented in PrecipHENS at large catchments, this is the case across the basin. The temporal correlation in Figure 16 is given at a lag of 1-day, and so Figure C3 provides a longer-term correlation example at a lag of 10 days. Again, the coherent patterns and structure across the basin are recovered in PrecipHENS for both the average and the extremes.

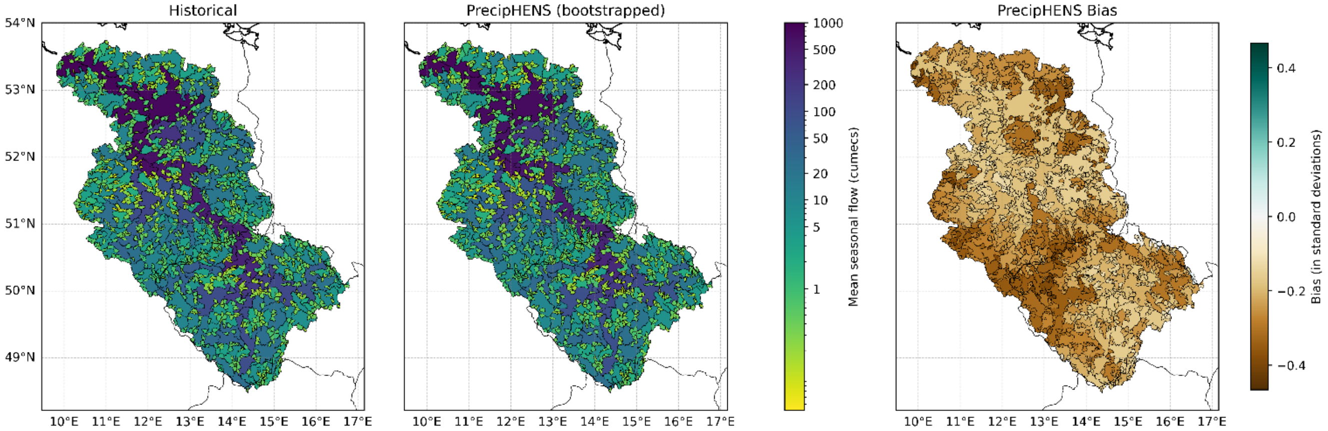

Figure C1: Mean seasonal river flow (in cumecs) for all catchments across the Elbe. See Figure 13 for caption details, which shows a subset of larger catchments.

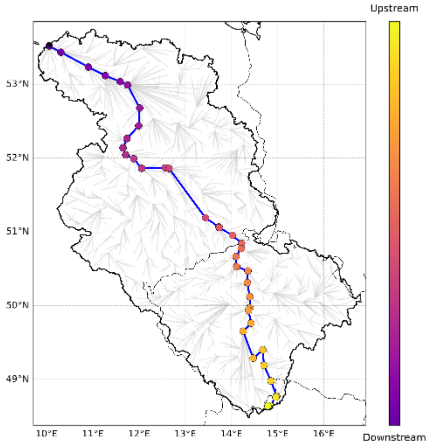

Figure C2: The catchments along the main trunk of the river Elbe, used in examples of Section 3.2 River flow generation results. The Elbe basin is highlighted with the grey lines showing the network connections between catchment outflow points across the basin. The outflow point of the catchments along the main trunk are shown with the points, coloured by the upstream-downstream positioning (this colour scale is used in relevant figures such as Figure 14).

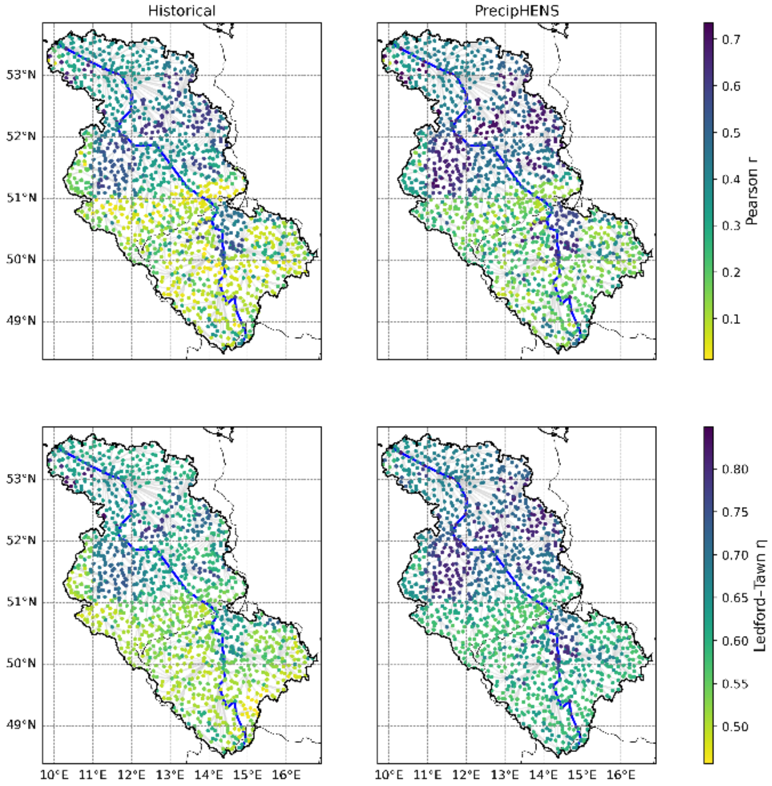

Figure C3: Correlation between daily river flow at each catchment and the flow at that respective catchment 10 days later (i.e., lag of 10 days), computed across the winter period. In each case, only the outflow point of the catchment is shown as a point, and the grey connections highlight the structure of the river network, with the main trunk of the Elbe highlighted in the blue line. Panels show results for historical data (left) and PrecipHENS simulations (right). Correlation is shown for all data with Pearson's r (top row) and for extreme correlation with Ledford–Tawn tail dependence coefficient (η) (bottom row, quantile threshold of 0.9).

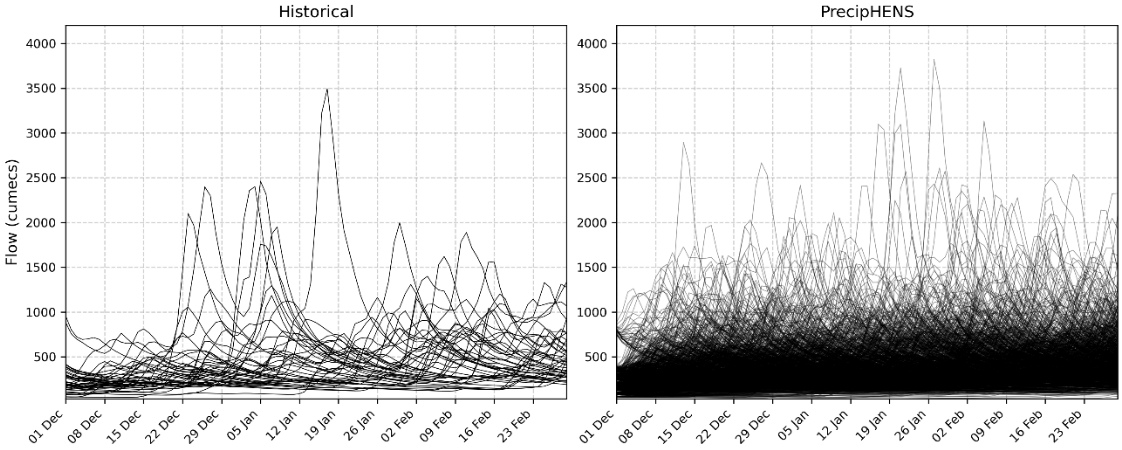

Figure C4: Full-season river flow simulations at the Dresden reference location. The historical data (left) are the modelled flows from all 43 historical precipitation seasons with their respective initial catchment conditions, while the PrecipHENS data (right) are each of the 1008 weather simulations paired with a random initial catchment condition (for visual clarity as opposed to all 43344 flow simulations).

Code availability

Due to its proprietary nature and competitive interest, the software code in its entirety cannot be made openly available. The individual AI models and their associated trained weights that form the PrecipHENS workflow (see Figure 3) are available under an Apache 2.0 license at https://github.com/NVIDIA/earth2studio (PhysicsNeMo Contributors, 2024). The GR4J hydrological model underlying the river results is available under an MIT license at https://github.com/kratzert/RRMPG (Čertík et al., 2022).

Data availability

A subset of the datasets can be shared for academic research purposes upon reasonable request. Interested researchers may contact the lead authors to request access.

Author contributions

Conceptualisation: J. Ashcroft (JA) and A. Poulston (AP)
Methodology: JA, AP, M. Koch (MK), and G. Ertl (GE)
Software: K. Brown (KB), J. Butler (JB), A. Hammond (AH), O. Jordan (OJ), and S. Warren (SW)
Writing – original draft: JA and AP
Writing – review and editing: all authors, with significant input from JA, AP, R. Lamb (RL), P. J. Young (PJY) and D. Wood (DW)

Competing interests

No authors have any competing interests.

Acknowledgements

The authors thank Dave Leedal, Valeriya Filipova, Douglas Burns, and Ashleigh Massam for their valuable insights during discussions on the meteorological and hydrological modelling. We are also grateful to Kathryn Madden, Barbara Nix, Farah Hariri and Jochen Papenbrock for their project management support. Finally, we acknowledge Ye Liu, Monika Leng, and John Paul Gosling, former colleagues whose earlier work provided an important foundation for this study.

References

Alexandre, D. A., Chaudhuri, C., and Gill-Fortin, J.: Novel extensions to the Fisher copula to model flood spatial dependence over North America, Hydrol. Earth Syst. Sci., 28, 5069–5085, https://doi.org/10.5194/hess-28-5069-2024, 2024.

Allaire, M.: Socio-economic impacts of flooding: A review of the empirical literature, Water Secur., 3, 18–26, https://doi.org/10.1016/j.wasec.2018.09.002, 2018.

Anon: Scalgo Hydrology, n.d.

Arino, O., Ramos Perez, J. J., Kalogirou, V., Bontemps, S., Defourny, P., and Van Bogaert, E.: Global Land Cover Map for 2009 (GlobCover 2009), https://doi.org/10.1594/PANGAEA.787668, 2012.

Bonev, B., Kurth, T., Hundt, C., Pathak, J., Baust, M., Kashinath, K., and Anandkumar, A.: Spherical Fourier Neural Operators: Learning Stable Dynamics on the Sphere, Proc. 40th Int. Conf. Mach. Learn., 202, 2806–2823, 2023.

Brocca, L., Melone, F., and Moramarco, T.: Distributed rainfall-runoff modelling for flood frequency estimation and flood forecasting, Hydrol. Process., 25, 2801–2813, https://doi.org/10.1002/hyp.8042, 2011.

Brunner, M. I. and Gilleland, E.: Stochastic simulation of streamflow and spatial extremes: a continuous, wavelet-based approach, Hydrol. Earth Syst. Sci., 24, 3967–3982, https://doi.org/10.5194/hess-24-3967-2020, 2020.

Brunner, M. I., Furrer, R., and Favre, A.-C.: Modeling the spatial dependence of floods using the Fisher copula, Hydrol. Earth Syst. Sci., 23, 107–124, https://doi.org/10.5194/hess-23-107-2019, 2019.

Brunner, M. I., Papalexiou, S., Clark, M. P., and Gilleland, E.: How Probable Is Widespread Flooding in the United States?, Water Resour. Res., 56, e2020WR028096, https://doi.org/10.1029/2020WR028096, 2020.

Čertík, O., Klotz, D., MacDonald, A., Visser, M., Gauch, M., and martinma10: Rainfall-Runoff modelling playground, 2022.

Cooley, D. and Thibaud, E.: Decompositions of dependence for high-dimensional extremes, Biometrika, 106, 587–604, https://doi.org/10.1093/biomet/asz028, 2019.

Cotterill, D. F., Mitchell, D., Stott, P. A., and Bates, P.: Using UNSEEN approach to attribute regional UK winter rainfall extremes, Int. J. Climatol., 44, 2406–2424, https://doi.org/10.1002/joc.8460, 2024.

CRESTA CLIX: CRESTA CLIX Press Release Q4 2024, PERILS AG, 2024.

Davison, A. C. and Smith, R. L.: Models for Exceedances Over High Thresholds, J. R. Stat. Soc. Ser. B Methodol., 52, 393–425, https://doi.org/10.1111/j.2517-6161.1990.tb01796.x, 1990.

Drees, H. and Sabourin, A.: Principal component analysis for multivariate extremes, Electron. J. Stat., 15, https://doi.org/10.1214/21-EJS1803, 2021.

European Environment Agency (EEA): European Digital Elevation Model (EU-DEM) (1.1), 2016.

Ferreira, C. S. S., Potočki, K., Kapović-Solomun, M., and Kalantari, Z.: Nature-Based Solutions for Flood Mitigation and Resilience in Urban Areas, in: Nature-Based Solutions for Flood Mitigation: Environmental and Socio-Economic Aspects, edited by: Ferreira, C. S. S., Kalantari, Z., Hartmann, T., and Pereira, P., Springer International Publishing, Cham, 59–78, https://doi.org/10.1007/698_2021_758, 2022.

Formetta, G., Svensson ,Cecilia, and and Stewart, E.: Spatio-temporal clustering of extreme floods in Great Britain, Hydrol. Sci. J., 69, 1288–1300, https://doi.org/10.1080/02626667.2024.2367167, 2024.

Gupta, H. V., Kling, H., Yilmaz, K. K., and Martinez, G. F.: Decomposition of the mean squared error and NSE performance criteria: Implications for improving hydrological modelling, J. Hydrol., 377, 80–91, https://doi.org/10.1016/j.jhydrol.2009.08.003, 2009.

Heffernan, J. E. and Tawn, J. A.: A conditional approach for multivariate extreme values (with discussion), J. R. Stat. Soc. Ser. B Stat. Methodol., 66, 497–546, https://doi.org/10.1111/j.1467-9868.2004.02050.x, 2004.

Hersbach, H., Bell, B., Berrisford, P., Hirahara, S., Horányi, A., Muñoz-Sabater, J., Nicolas, J., Peubey, C., Radu, R., Schepers, D., Simmons, A., Soci, C., Abdalla, S., Abellan, X., Balsamo, G., Bechtold, P., Biavati, G., Bidlot, J., Bonavita, M., De Chiara, G., Dahlgren, P., Dee, D., Diamantakis, M., Dragani, R., Flemming, J., Forbes, R., Fuentes, M., Geer, A., Haimberger, L., Healy, S., Hogan, R. J., Hólm, E., Janisková, M., Keeley, S., Laloyaux, P., Lopez, P., Lupu, C., Radnoti, G., De Rosnay, P., Rozum, I., Vamborg, F., Villaume, S., and Thépaut, J.: The ERA5 global reanalysis, Q. J. R. Meteorol. Soc., 146, 1999–2049, https://doi.org/10.1002/qj.3803, 2020.

Hijmans, R. J., Cameron, S. E., Parra, J. L., Jones, P. G., and Jarvis, A.: Very high resolution interpolated climate surfaces for global land areas, Int. J. Climatol., 25, 1965–1978, https://doi.org/10.1002/joc.1276, 2005.

Karlbauer, M., Cresswell-Clay, N., Durran, D. R., Moreno, R. A., Kurth, T., Bonev, B., Brenowitz, N., and Butz, M. V.: Advancing Parsimonious Deep Learning Weather Prediction Using the HEALPix Mesh, J. Adv. Model. Earth Syst., 16, e2023MS004021, https://doi.org/10.1029/2023MS004021, 2024.

Kay, A. L., Booth, N., Lamb, R., Raven, E., Schaller, N., and Sparrow, S.: Flood event attribution and damage estimation using national-scale grid-based modelling: Winter 2013/2014 in Great Britain, Int. J. Climatol., 38, 5205–5219, https://doi.org/10.1002/joc.5721, 2018.

Keef, C., Svensson, C., and Tawn, J. A.: Spatial dependence in extreme river flows and precipitation for Great Britain, J. Hydrol., 378, 240–252, https://doi.org/10.1016/j.jhydrol.2009.09.026, 2009.

Keef, C., Tawn, J. A., and Lamb, R.: Estimating the probability of widespread flood events, Environmetrics, 24, 13–21, https://doi.org/10.1002/env.2190, 2013.

Klingler, C., Schulz, K., and Herrnegger, M.: LamaH-CE: LArge-SaMple DAta for Hydrology and Environmental Sciences for Central Europe, Earth Syst. Sci. Data, 13, 4529–4565, https://doi.org/10.5194/essd-13-4529-2021, 2021.

Kottek, M., Grieser, J., Beck, C., Rudolf, B., and Rubel, F.: World Map of the Köppen-Geiger climate classification updated, Meteorol. Z., 15, 259–263, https://doi.org/10.1127/0941-2948/2006/0130, 2006.

Kunnath-Poovakka, A. and Eldho, T. I.: A comparative study of conceptual rainfall-runoff models GR4J, AWBM and Sacramento at catchments in the upper Godavari river basin, India, J. Earth Syst. Sci., 128, 33, https://doi.org/10.1007/s12040-018-1055-8, 2019.

Lamb, R., Keef, C., Tawn, J., Laeger, S., Meadowcroft, I., Surendran, S., Dunning, P., and Batstone, C.: A new method to assess the risk of local and widespread flooding on rivers and coasts, J. Flood Risk Manag., 3, 323–336, https://doi.org/10.1111/j.1753-318X.2010.01081.x, 2010.

Lamb, R., Garside, P., Pant, R., and Hall, J. W.: A Probabilistic Model of the Economic Risk to Britain's Railway Network from Bridge Scour During Floods, Risk Anal., 39, 2457–2478, https://doi.org/10.1111/risa.13370, 2019.

Lamb, R., Longfield, S., Manson, S., Cloke, H. L., Pilling, C., Reynard, N., Sheppard, O., Asadullah, A., Vaughan, M., Fowler, H. J., and Beven, K. J.: The future of flood hydrology in the UK, Hydrol. Res., 53, 1286–1303, https://doi.org/10.2166/nh.2022.053, 2022.

Ledford, A. and Tawn, J. A.: Statistics for near independence in multivariate extreme values, Biometrika, 83, 169–187, https://doi.org/10.1093/biomet/83.1.169, 1996.

Lee, D. and Joe, H.: Multivariate extreme value copulas with factor and tree dependence structures, Extremes, 21, 147–176, https://doi.org/10.1007/s10687-017-0298-0, 2018.

Li, H., Haer, T., Couasnon, A., Enríquez, A. R., Muis, S., and Ward, P. J.: A spatially-dependent synthetic global dataset of extreme sea level events, Weather Clim. Extrem., 41, 100596, https://doi.org/10.1016/j.wace.2023.100596, 2023.

Mahesh, A., Collins, W., Bonev, B., Brenowitz, N., Cohen, Y., Elms, J., Harrington, P., Kashinath, K., Kurth, T., North, J., OBrien, T., Pritchard, M., Pruitt, D., Risser, M., Subramanian, S., and Willard, J.: Huge Ensembles Part I: Design of Ensemble Weather Forecasts using Spherical Fourier Neural Operators, http://arxiv.org/abs/2408.03100, 6 August 2024a.

Mahesh, A., Collins, W., Bonev, B., Brenowitz, N., Cohen, Y., Harrington, P., Kashinath, K., Kurth, T., North, J., OBrien, T., Pritchard, M., Pruitt, D., Risser, M., Subramanian, S., and Willard, J.: Huge Ensembles Part II: Properties of a Huge Ensemble of Hindcasts Generated with Spherical Fourier Neural Operators, https://doi.org/10.48550/arXiv.2408.01581, 2 August 2024b.

Merz, B. and Thieken, A. H.: Flood risk curves and uncertainty bounds, Nat. Hazards, 51, 437–458, https://doi.org/10.1007/s11069-009-9452-6, 2009.

Merz, B., Aerts, J., Arnbjerg-Nielsen, K., Baldi, M., Becker, A., Bichet, A., Blöschl, G., Bouwer, L. M., Brauer, A., Cioffi, F., Delgado, J. M., Gocht, M., Guzzetti, F., Harrigan, S., Hirschboeck, K., Kilsby, C., Kron, W., Kwon, H.-H., Lall, U., Merz, R., Nissen, K., Salvati, P., Swierczynski, T., Ulbrich, U., Viglione, A., Ward, P. J., Weiler, M., Wilhelm, B., and Nied, M.: Floods and climate: emerging perspectives for flood risk assessment and management, https://doi.org/10.5194/nhessd-2-1559-2014, 14 February 2014.

Mitchell-Wallace, K., Jones, M., Hillier, J., and Foote, M. (Eds.): Natural catastrophe risk management and modelling: A practitioner's guide, John Wiley and Sons, Inc, Hoboken, NJ, 2017.

Nied, M., Hundecha, Y., and Merz, B.: Flood-initiating catchment conditions: a spatio-temporal analysis of large-scale soil moisture patterns in the Elbe River basin, Hydrol. Earth Syst. Sci., 17, 1401–1414, https://doi.org/10.5194/hess-17-1401-2013, 2013.

Olcese, G., Bates, P. D., Neal, J. C., Sampson, C. C., Wing, O. E. J., Quinn, N., Murphy-Barltrop, C. J. R., and Probyn, I.: Developing a Fluvial and Pluvial Stochastic Flood Model of Southeast Asia, Water Resour. Res., 60, e2023WR036580, https://doi.org/10.1029/2023WR036580, 2024.

Oudin, L., Hervieu, F., Michel, C., Perrin, C., Andréassian, V., Anctil, F., and Loumagne, C.: Which potential evapotranspiration input for a lumped rainfall–runoff model?: Part 2—Towards a simple and efficient potential evapotranspiration model for rainfall–runoff modelling, J. Hydrol., 303, 290–306, https://doi.org/10.1016/j.jhydrol.2004.08.026, 2005.

Pathak, J., Subramanian, S., Harrington, P., Raja, S., Chattopadhyay, A., Mardani, M., Kurth, T., Hall, D., Li, Z., Azizzadenesheli, K., Hassanzadeh, P., Kashinath, K., and Anandkumar, A.: FourCastNet: A Global Data-driven High-resolution Weather Model using Adaptive Fourier Neural Operators, http://arxiv.org/abs/2202.11214, 22 February 2022.

Pearson, K.: Notes on regression and inheritance in the case of two parents, in: Proceedings of the Royal Society of London, Taylor & Francis, 1895.

Perrin, C., Michel, C., and Andréassian, V.: Improvement of a parsimonious model for streamflow simulation, J. Hydrol., 279, 275–289, https://doi.org/10.1016/S0022-1694(03)00225-7, 2003.

PhysicsNeMo Contributors: NVIDIA Earth2Studio, 2024.

Politis, D. N. and and Romano, J. P.: The Stationary Bootstrap, J. Am. Stat. Assoc., 89, 1303–1313, https://doi.org/10.1080/01621459.1994.10476870, 1994.

Quinn, N., Bates, P. D., Neal, J., Smith, A., Wing, O., Sampson, C., Smith, J., and Heffernan, J.: The Spatial Dependence of Flood Hazard and Risk in the United States, Water Resour. Res., 55, 1890–1911, https://doi.org/10.1029/2018WR024205, 2019.

Rohrbeck, C. and Cooley, D.: Simulating flood event sets using extremal principal components, http://arxiv.org/abs/2106.00630, 16 March 2022.

Sando, K., Wada, R., Rohmer, J., and Jonathan, P.: Multivariate spatial and spatio-temporal models for extreme tropical cyclone seas, Ocean Eng., 309, 118365, https://doi.org/10.1016/j.oceaneng.2024.118365, 2024.

Schaller, N., Kay, A. L., Lamb, R., Massey, N. R., van Oldenborgh, G. J., Otto, F. E. L., Sparrow, S. N., Vautard, R., Yiou, P., Ashpole, I., Bowery, A., Crooks, S. M., Haustein, K., Huntingford, C., Ingram, W. J., Jones, R. G., Legg, T., Miller, J., Skeggs, J., Wallom, D., Weisheimer, A., Wilson, S., Stott, P. A., and Allen, M. R.: Human influence on climate in the 2014 southern England winter floods and their impacts, Nat. Clim. Change, 6, 627–634, https://doi.org/10.1038/nclimate2927, 2016.

Shepherd, T. G., Boyd, E., Calel, R. A., Chapman, S. C., Dessai, S., Dima-West, I. M., Fowler, H. J., James, R., Maraun, D., Martius, O., Senior, C. A., Sobel, A. H., Stainforth, D. A., Tett, S. F. B., Trenberth, K. E., van den Hurk, B. J. J. M., Watkins, N. W., Wilby, R. L., and Zenghelis, D. A.: Storylines: an alternative approach to representing uncertainty in physical aspects of climate change, Clim. Change, 151, 555–571, https://doi.org/10.1007/s10584-018-2317-9, 2018.

Shin, M.-J. and Kim, C.-S.: Assessment of the suitability of rainfall–runoff models by coupling performance statistics and sensitivity analysis, Hydrol. Res., 48, 1192–1213, https://doi.org/10.2166/nh.2016.129, 2017.

https://doi.org/10.5194/egusphere-2025-5841
Preprint. Discussion started: 9 December 2025

Steirou, E., Gerlitz, L., Sun, X., Apel, H., Agarwal, A., Totz, S., and Merz, B.: Towards seasonal forecasting of flood probabilities in Europe using climate and catchment information, Sci. Rep., 12, 13514, https://doi.org/10.1038/s41598-022-16633-1, 2022.

Svetlana, D., Radovan, D., and Ján, D.: The Economic Impact of Floods and their Importance in Different Regions of the World with Emphasis on Europe, Procedia Econ. Finance, 34, 649–655, https://doi.org/10.1016/S2212-5671(15)01681-0, 2015.

Tawn, J., Shooter, R., Towe, R., and Lamb, R.: Modelling spatial extreme events with environmental applications, Spat. Stat., 28, 39–58, https://doi.org/10.1016/j.spasta.2018.04.007, 2018.

Thornton, J., Smith, H., Leedal, D., Young, P., Charge, J., Filipova, V., Hannah Kellett, Lamb, R., and Waller, S.: High-resolution inland flood hazard quantification for any country: The JBA framework and example applications.

Toth, Z. and Kalnay, E.: Ensemble Forecasting at NMC: The Generation of Perturbations, Bull. Am. Meteorol. Soc., 74, 2317–2330, https://doi.org/10.1175/1520-0477(1993)074%253C2317:EFANTG%253E2.0.CO;2, 1993.

Toth, Z. and Kalnay, E.: Ensemble Forecasting at NCEP and the Breeding Method, Mon. Weather Rev., 125, 3297–3319, https://doi.org/10.1175/1520-0493(1997)125%253C3297:EFANAT%253E2.0.CO;2, 1997.

Towe, R., Tawn, J., and Lamb, R.: Why Extreme Floods are More Common than you Might Think, Significance, 15, 16–21, https://doi.org/10.1111/j.1740-9713.2018.01209.x, 2018.

Tyler, J., Sadiq, A.-A., and Noonan, D. S.: A review of the community flood risk management literature in the USA: lessons for improving community resilience to floods, Nat. Hazards, 96, 1223–1248, https://doi.org/10.1007/s11069-019-03606-3, 2019.

Valéry, A., Andréassian, V., and Perrin, C.: 'As simple as possible but not simpler': What is useful in a temperature-based snow-accounting routine? Part 1 – Comparison of six snow accounting routines on 380 catchments, J. Hydrol., 517, 1166–1175, https://doi.org/10.1016/j.jhydrol.2014.04.059, 2014a.

Valéry, A., Andréassian, V., and Perrin, C.: 'As simple as possible but not simpler': What is useful in a temperature-based snow-accounting routine? Part 2 – Sensitivity analysis of the Cemaneige snow accounting routine on 380 catchments, J. Hydrol., 517, 1176–1187, https://doi.org/10.1016/j.jhydrol.2014.04.058, 2014b.

Van De Vyver, H.: Fast generation of high-dimensional spatial extremes, Weather Clim. Extrem., 46, 100732, https://doi.org/10.1016/j.wace.2024.100732, 2024.

Wang, R., Liu, J., and Wang, J.: The extremal spatial dependence of significant wave height in the South China sea, Ocean Eng., 295, 116888, https://doi.org/10.1016/j.oceaneng.2024.116888, 2024.

Xu, W., Chen, K., Han, T., Chen, H., Ouyang, W., and Bai, L.: ExtremeCast: Boosting Extreme Value Prediction for Global Weather Forecast, https://doi.org/10.48550/arXiv.2402.01295, 16 August 2024.

Zanardo, S. and Salinas, J. L.: An introduction to flood modeling for catastrophe risk management, WIREs Water, 9, e1568, https://doi.org/10.1002/wat2.1568, 2022.

Zhang, Y., Li, Z., Xu, H., Ge, W., Qian, H., Li, J., Sun, H., Zhang, H., and Jiao, Y.: Impact of floods on the environment: A review of indicators, influencing factors, and evaluation methods, Sci. Total Environ., 951, 175683, https://doi.org/10.1016/j.scitotenv.2024.175683, 2024.

890 Zobler, L.: Global Soil Types, 1-degree grid, https://doi.org/10.3334/ORNLDAAC/418, 1999.